Biogeosciences Discuss., https://doi.org/10.5194/bg-2018-340
Manuscript under review for journal Biogeosciences
Discussion started: 2 August 2018

Vivianite formation in methane-rich deep-sea sediments from the South China Sea

Jiarui Liu[1], Jiasheng Wang[1], Gareth Izon[2], Gilad Antler[3,4,5], Zhou Wang[1], Jie Zhao[1], Matthias Egger[6]

[1] State Key Laboratory of Biogeology and Environment Geology, College of Marine Science and Technology, School of Earth Sciences, China University of Geosciences, Wuhan, 430074, China
[2] Department of Earth, Atmospheric and Planetary Sciences, Massachusetts Institute of Technology, Cambridge, MA, 02139, USA
[3] Department of Earth Sciences, University of Cambridge, Cambridge, CB2 3EQ, UK
[4] Department of Geological and Environmental Sciences, Ben-Gurion University of the Negev, Beersheba, 84105, Israel
[5] The Interuniversity Institute for Marine Sciences, Eilat, 88103, Israel
[6] The Ocean Cleanup Foundation, Rotterdam, 3014 JH, the Netherlands

Correspondence to: Jiasheng Wang (js-wang@cug.edu.cn)

Abstract. Phosphorus is often invoked as the ultimate limiting nutrient, modulating primary productivity on geological timescales. Consequently, along with nitrogen, phosphorus bioavailability exerts a fundamental control on organic carbon production, linking all the biogeochemical cycles across the Earth system. Unlike nitrogen that can be microbially fixed from an essentially infinite atmospheric reservoir, phosphorus availability is dictated by the interplay between its sources and sinks. While authigenic apatite formation has received considerable attention as the dominant sedimentary phosphorus sink, the quantitative importance of reduced iron-phosphate minerals, such as vivianite, has only recently been acknowledged and their importance remains under-explored. Combining microscopic and spectroscopic analyses of handpicked mineral aggregates with sediment geochemical profiles we characterize the distribution and mineralogy of iron-phosphate minerals present in methane-rich sediments recovered from the northern South China Sea. Here, we demonstrate that vivianite authigenesis is pervasive in the iron oxide-rich sediments below the sulfate-methane transition zone (SMTZ). We hypothesize that the downward migration of the SMTZ concentrated vivianite formation below the current SMTZ. Our observations support recent findings from non-steady state post-glacial coastal sedimentary successions, suggesting that iron reduction below the SMTZ, probably driven by iron-mediated anaerobic oxidation of methane (Fe-AOM), is coupled to phosphorus cycling on a much greater spatial scale than previously assumed. Calculations reveal that vivianite acts as an important burial phase for both iron and phosphorus below the SMTZ, sequestering approximately half of the total reactive iron pool. By extension, sedimentary vivianite formation could serve as a mineralogical marker of Fe-AOM, signalling a low-sulfate availability against methanogenic and ferruginous backdrop. Given that similar conditions were likely present throughout vast swaths of Earth history, it is possible that Fe-AOM may have modulated phosphorus and methane availability on the early Earth.

Biogeosciences Discuss., https://doi.org/10.5194/bg-2018-340
Manuscript under review for journal Biogeosciences
Discussion started: 2 August 2018

1 Introduction

Phosphorus (P) is an essential nutrient, and its availability limits primary production on both short and long timescales (Algeo and Ingall, 2007; Ruttenberg, 2014). Marine sediments are known to regulate water column P availability, either retaining or releasing P dependent on the prevailing redox conditions (Delaney, 1998; Slomp et al., 1996). Phosphate is mainly present as HPO_4^{2-} in seawater (henceforth termed PO_4), which is captured and shuttled to the seabed in association with organic debris (organic P) or adsorbed onto iron (Fe)-(oxyhydr)oxides (hence after termed Fe-oxide bound P). Through a combination of organic matter remineralization and reductive dissolution of Fe-oxides, PO_4 is released to the sediment pore water where successive precipitation of P-bearing minerals can sequester P for potentially geologically relevant timescales (Jensen et al., 1995; Ruttenberg and Berner, 1993; Sundby et al., 1992). Authigenic carbonate fluorapatite (CFA) is typically assumed to be the dominant sedimentary P mineral, accounting for around half of global marine P burial (Ruttenberg, 2014). Another potentially important group of P burial phases that have only recently been recognized are Fe(II)-phosphate minerals, such as vivianite ($Fe_3(PO_4)_2 \cdot 8H_2O$). The importance of Fe(II)-phosphate minerals, however, is not completely known.

Vivianite authigenesis requires pore water with elevated ferrous iron (Fe^{2+}) and PO_4 concentrations. Low-sulfate lacustrine settings typically satisfy these criteria, and vivianite has commonly been reported in freshwater sediments (e.g., Fagel et al., 2005; Rothe et al., 2014; Sapota et al., 2006). In more sulfate-rich settings, the presence of a sulfate-methane transition zone (SMTZ) has been shown to provide favorable conditions for sedimentary vivianite authigenesis (Egger et al., 2015a, 2016; Hsu et al., 2014; März et al., 2008; Slomp et al., 2013). The production of dissolved sulfide by sulfate-dependent anaerobic oxidation of methane (SO_4-AOM) in the SMTZ and the associated conversion of Fe-oxides to Fe-sulfides results in elevated pore water PO_4 concentrations around the SMTZ. The subsequent downward diffusion of PO_4 into sulfide-depleted pore water below the SMTZ can then lead to the precipitation of vivianite, provided that sufficient reduced Fe is available at depth. Possible sources of Fe^{2+} below the SMTZ are organoclastic Fe reduction, abiotic reductive dissolution of ferric-phases by sulfide, anaerobic oxidation of methane coupled to the reduction of ferric Fe (Fe-AOM), as well as more cryptic and less well understood mechanisms (Egger et al., 2017 and references therein). Of these, Fe-AOM is often suggested as the most likely mechanism, supplying plentiful Fe^{2+} at the expense of methane due to the 8:1 stoichiometric conversion of Fe to methane (Eq. 1; Amos et al., 2012; Beal et al., 2009; Crowe et al., 2011; Egger et al., 2015b, 2016, 2017; Norði et al., 2013; Riedinger et al., 2014; Segarra et al., 2013; Sivan et al., 2011; Wankel et al., 2012).

$$CH_4 + 8Fe(OH)_3 + 15H^+ \rightarrow HCO_3^- + 8Fe^{2+} + 21H_2O \quad \text{(Eq.1)}$$

Iron-mediated AOM can be performed by anaerobic methane oxidizing archaea (ANME) who oxidize methane nonsyntropically, exploiting soluble and nanophase ferric iron (Fe^{3+}) as electron acceptors (Ettwig et al., 2016; Scheller et al., 2016). The presence of large multi-haem cytochromes (proteins that mediate electron transport) and type IV pili (cellular appendages) detected in the genomes of ANME hint that these archaea may also exploit solid Fe-oxides via extracellular electron transport (McGlynn et al., 2015; Wegener et al., 2015). The experimental approach of Bar-Or et al. (2017) further demonstrates that more refractory reactive Fe-oxides (e.g., magnetite and hematite) could also serve as electron acceptors for

Fe-AOM. While the biochemical investigation of *Methanosarcina activorans* has illuminated the mechanistics of Fe-AOM (Yan et al., 2018), the modes and pathways of Fe-AOM remain enigmatic and warrant further exploration.

Vivianite authigenesis, potentially fueled by Fe-AOM, couples the biogeochemical cycles of Fe, P, sulfur (S) and carbon (C) in the deep biosphere. Consequently, given the importance of these elemental cycles within the Earth System, knowledge about vivianite precipitation and preservation in marine sediments is essential. While the database of vivianite occurrence in marine systems is growing, most of these records are from sites with atypical and time variable stratigraphic records. For example, much of work to-date has focused on vivianite authigenesis in non-steady state post-glacial sedimentary successions from marginal basins like the Baltic and Black Seas (Dijkstra et al., 2016, 2018a, 2018b; Egger et al., 2015a; Reed et al., 2016). In these settings, post-glacial sea-level rise resulted in the accumulation of organic rich sediments overlying organic-poor lacustrine deposits, which is far from representative of typical marine sedimentation. Other reports of possible vivianite formation in marine systems are from deep sea fan sediments (Burns, 1997; März et al., 2008), as well as from accretionary wedge sediments (Hsu et al., 2014). A more detailed understanding of vivianite authigenesis and the interplay between CH_4, S, Fe and P in open marine sediments will improve our ability to read ancient sediment records and to potentially test hypotheses linking nutrient availability, climate and biospheric evolution.

In this study, we combine microscopic and spectroscopic analyses of handpicked mineral aggregates with bulk geochemical analyses to characterize the distribution and mineralogy of Fe-phosphate minerals in the methane-rich deep-sea sediments preserved in the Taixinan Basin, northern South China Sea (Fig. 1). X-ray diffraction and down core abundance records reveal vivianite authigenesis in this open marine sedimentary system. We further discuss the pathways for vivianite authigenesis below the SMTZ and the role of anaerobic methane oxidation. Our results support recent findings that vivianite formation can be an important burial mechanism for Fe and P at depth in methane-rich marine sediments, indicating that vivianite authigenesis may have been more pervasive in the Earth's past.

2 Geological background and study site

The Taixinan (or Southwestern Taiwan) Basin is located east of the northern continental slope of the South China Sea (Fig. 1) and separates a passive margin and an active accretionary wedge (Liu et al., 1997). As a Cenozoic hydrocarbon-bearing sedimentary basin featuring 1–3 km of sediment accumulation, the Taixinan Basin represents a promising area for gas hydrate and cold seep exploration (McDonnell et al., 2000). For example, a large seep-induced carbonate buildup (Jiulong Methane Reef, Site 1–3), covering about 430 km^2, was discovered during the R/V *SONNE* Cruise SO-177 in 2004 (Han et al., 2008; Suess et al., 2005). East of these inactive seeps, Site F on the Formosa Ridge represents one of the most vigorous cold seeps reported from within the South China Sea, supporting a large and diverse chemosynthetic ecosystem (Feng and Chen, 2015; Feng et al., 2015; Hsu et al., 2017). Massive gas hydrates were recovered during China's second major gas hydrate expedition (GMGS-2) in 2013 (Sha et al., 2015; Zhang et al., 2015b), which further confirms that gas hydrate and seepage of methane-rich fluids are well developed in the Taixinan Basin.

A piston core (total length of 13.85 m) was taken at Site 973-4 (118°49' E, 21°54' N) in 2011 during a cruise with R/V *Ocean VI* (Fig. 1). Retrieved from the lower continental slope at a water depth of 1666 m, core 973-4 is dominated by dark-green silty clay. The only deviation in grain-size is seen in a siltier layer between 455−605 cm depth, whose coarse fraction (> 65 μm) increases in association with increased abundances of foraminifera and Fe-rich silicates (Fig. 2a). Radiocarbon- and $\delta^{18}O$-derived age models (Fig. 2a) suggest sedimentation rates were relatively constant (32 cm ka^{-1}) throughout the ~40-thousand-years (ka) of deposition encompassed by core 973-4. Again, the only departure is associated with the coarser layer during the Last Glacial Maximum, which yields atypically old radiocarbon ages relative to the surrounding sediment. This observation is consistent with the frequent slumping and/or turbidity currents influencing this area (e.g., Zhong et al., 2015), which might in turn reflect destabilization of gas hydrates on the upper continental slope and subsequent continental-slope failure during sea-level low stands (Kennett et al., 2003; Maslin et al., 2004).

3. Methods

After retrieval, the core was cut into sections and transferred to a cold room where it was stored below 4 °C. Each sample was divided into two subsamples. The first subsample was used to isolate specific mineral phases via conventional handpicking (Lin et al., 2016a) and the second subsample was used for chemical analyses. After drying at 60 °C for 24 h, the sediments were sieved with distilled water allowing the coarse fraction (> 65 μm) to be collected. Mineral aggregates were then identified and handpicked from the greater than 65 μm fraction (coarse component) under a stereomicroscope. The weight of these mineral fractions, along with the coarse component of the sediments, were determined and their concentrations were expressed relative to the initial dry mass of the sample.

The morphology and chemical composition of the handpicked minerals were investigated using a FEI Quanta 450 FEG scanning electron microscope (SEM) in energy dispersive spectroscopy (EDS) mode. Power X-ray diffraction (XRD) analysis of the handpicked samples was performed using Ni-filtered Cu Kα radiation on a Panalytical X'Pert Pro diffractometer. The X-ray diffractometer was operated at 40 kV and 40 mA over a 3–65° 2θ range. The analytical step size was 0.017° with a measurement dwell time of 0.4 s per step. Raman analysis of the handpicked samples was performed by a JY/Horiba LabRam HR Raman system, using 532.06 nm (frequency doubled Nd:YAG) laser excitation, a 50× Olympus objective, and a 300-groove/mm grating.

Two different operationally defined solid-phase Fe pools were determined chemically on separate aliquots of freeze-dried sample (e.g., Holmkvist et al., 2014). Briefly, the most readily acid-soluble Fe minerals, including ferrihydrite and lepidocrocite, were extracted via agitation in an anoxic 0.5 M HCl solution for one hour. The Fe(II) content of this extract was then determined via the 1, 10-phenanthroline method (Amonette and Templeton, 1998), followed by the total Fe content (i.e., Fe(II) + Fe(III)) with a 1, 10-phenanthroline and 1% (w/v) hydroxylamine hydrochloride assay. Poorly crystalline Fe(III) (oxy)hydroxides were then calculated as the difference between the reduced and mixed-valence Fe determinations. More crystalline Fe-oxides, including goethite, hematite and part of the poorly reactive sheet silicate Fe fraction, were then quantified

after treating a separate sample aliquot with a mixed dithionite-citrate-acetic acid solution for two hours (Poulton and Canfield, 2005). The Fe(III) and manganese (Mn) contents of the supernatant were measured by flame atomic absorption spectrometry (Pgeneral, TAS-990) with relative standard deviations (RSD) of better than 5%. These elemental fractions were termed reactive Fe-oxides and reactive Mn, respectively.

Due to unforeseen circumstances pore water was not extracted upon core recovery, but was delayed by several months following the cruise, compromising the available pore water methane and sulfate profiles (Zhang et al., 2014). Fortunately, pore water sulfate and methane concentrations are relatively well constrained from proximal sites (Lin et al., 2017b; Lu et al., 2012; Ye et al., 2016). The pore water chemistry of these nearby sites displays consistently shallow SMTZs, found between 700 and 880 cm depth, fueled by a high methane flux released from underlying gas hydrates (Sha et al., 2015). Where necessary, we therefore adopt data from a compilation of adjacent sites to constrain the position of the SMTZ (Fig. 2b).

4. Results

4.1 Morphology and chemical composition of mineral aggregates

Two types of dark mineral aggregates were identified. Examination of these handpicked mineral aggregates under a stereomicroscope revealed that the opaque blue to black crystals (0.1–1 µm diameter) were only present in samples below ~920 cm sediment depth (Fig. 3a). By contrast, stereomicroscope and SEM observations showed that pyrite is pervasive throughout the upper part of the core, observed in samples both within and above the SMTZ. Moreover, SEM observations of the blue to black mineral phase found below the SMTZ disclosed a distinctive morphology, displaying spherical aggregates of radiating lath-, platy- and needle-shaped crystals (Figs. 3b−e, g). This distinct morphology strongly resembles vivianite crystals identified from the Baltic Sea (Dijkstra et al., 2016; Egger et al., 2015a) and lacustrine sediments (Rothe et al., 2014, 2015). Major peaks of O, Fe, P were observed in the EDS spectra of the blue to black aggregates (Fig. 3f), constituting 39%, 28%, and 19% of the aggregates by mass (n=12), respectively. The O, Fe, P mass-ratios and the mole Fe/P ratio (0.83) from EDS analyses also approximate those reported from sedimentary vivianite from the Bothnian Sea (0.82 and 0.86), as well as synthesized vivianite (0.99; Egger et al., 2015a). Additional minor peaks of Mg, Si, Al, Ca, Mn, S were also observed in the EDS spectra, constituting 4.9%, 1.8%, 1.6%, 1.6%, 1.2%, 1.2% of the aggregates by mass (n=12), respectively. The Fe–Mg–Mn ternary plot of these aggregates (Fig. 4) reveals that the Fe/(Fe+Mg) ratios range from ~0.64 to 0.98, while the Mn/(Mn+Fe) ratios range from ~0 to 0.05. These observations are similar to the high-Mg, low-Mn vivianite identified in the sediments recovered from offshore southwestern Taiwan (Hsu et al., 2014).

Additional grey to green mineral aggregates were observed in samples throughout the sediment core. These particles feature smooth surfaces (Fig. 3h), while their EDS spectra show high intensity Fe, Si, O peaks (Fig. 3i), suggesting an Fe-rich silicate phase.

4.2 XRD and Raman analyses of mineral aggregates

X-ray diffraction analyses confirm that the blue to black mineral aggregates found below the SMTZ are vivianite nodules (Fig. 5a). The high intensity narrow peak observed at 13.2° typifies XRD spectra obtained from both natural and synthetic vivianite crystals (Dijkstra et al., 2016; Egger et al., 2015a; Grizelj et al., 2017; Rothe et al., 2014). Other Mg- or Fe-bearing phosphate minerals such as metavivianite were not recognized in diffractograms of our samples. Raman analyses showed a curved baseline with broad peaks (Fig. 5c), potentially caused by fluorescence interference from the samples (Kagan and McCreery, 1994). Despite these limitations, some peaks can still be recognized, especially the peak around 1000 cm^{-1}. These spectral features are also consistent with the Raman spectra of vivianite crystals (Piriou and Poullen, 1984), and thus offer an additional line of evidence supporting the results obtained from SEM–EDS and XRD analyses.

The grey to green mineral aggregates are mainly composed of chlorite, illite, quartz, and albite. Additional peaks including orthoclase, siderite, calcite, dolomite, pyrite and vivianite were also identified (Figs. 5b and 6). The XRD spectra indicated that some illite peaks might belong to mixed-layer illite/smectite. Glauconite is a green Fe-rich member of illite group and is an abundant authigenic mineral at water depths between 30 and 2000 m (Porrenga, 1967). Considering its EDS spectra, with high intensity Fe, Si, O peaks, it is likely that the illite-group minerals identified in core 973-4 may include a considerable glauconite component. Besides Fe-rich illite, or possibly even glauconite, chlorite is another Fe-rich sheet silicate that would also give similar EDS spectra. Given the difficulties in distinguishing between low abundance Fe-rich clays in complex marine sediments by XRD, the grey to green mineral aggregates are simply referred to as Fe-rich silicates from here on.

4.3 Down-core variations of mineral aggregates

The distribution of authigenic minerals at Site 973-4 displays distinct down-core variability, especially at and around the SMTZ. High amounts of coarse grained pyrite were observed between ~560–880 cm sediment depth with a peak around the SMTZ. Handpicked vivianite aggregates were only identified between ~920–1370 cm depth in the sediment (Fig. 7a). The concentration of vivianite ranges from 0.02 wt.‰ to 1.58 wt.‰ directly below the SMTZ (920–1175 cm depth), decreasing to lower values (0 to 0.36 wt.‰) towards the base of the core (1175–1370 cm depth). Dark laminations and reddish-brown nodules are prominent between 892–904 cm depth where acid volatile sulfur (AVS) displays a sharp peak at the base of the SMTZ (Fig. 9b). Major peaks of O and Fe were observed in the EDS spectra of these nodules, while lower intensity S peaks were only observed in a few samples. Nodules of AVS usually turn reddish-brown during post-sampling oxidation, thus most of these nodules found at the base of the SMTZ are most likely oxidation products of AVS.

Iron-rich silicates were distributed throughout the core (Fig. 7b), displaying a peak between 455–605 cm sediment depth. This layer has an elevated coarse-grained component and is associated with atypically old radiocarbon ages (Fig. 2a). The XRD spectra reveal that the Fe-rich silicates within this layer include more chlorite, differing from the composition of background Fe-rich silicates (Fig. 6). Compared with the high abundances of Fe-rich silicates observed above (8.48 wt.%) and below (2.94

wt.%) the SMTZ, the abundance of Fe-rich silicates within the SMTZ is servilely diminished, ranging from 0.01 wt.% to 0.16 wt.%.

4.4 Solid phase iron and manganese geochemistry

Ferric iron minerals were quantified using two different extraction methods. Both approaches yielded broadly consistent trends (Fig. 8a). The absolute concentrations of Fe (oxy)hydroxides and reactive Fe-oxides are low both immediately above and within the SMTZ, reaching a minimum of 34 µmol g^{-1} and 76 µmol g^{-1} within the more silty layer, respectively. Their concentrations increase to 173 µmol g^{-1} and 238 µmol g^{-1} at 900 cm depth and remain high around 123–161 µmol g^{-1} and 174–235 µmol g^{-1} below the SMTZ, respectively (Fig. 8a). Since more crystalline Fe minerals (e.g. goethite, hematite) are extracted by dithionite-citrate-acetic acid solution (Poulton and Canfield, 2005; Raiswell et al., 1994), the concentrations of reactive Fe-oxides are higher than those of Fe (oxy)hydroxides throughout the core. Therefore, for simplicity, reactive Fe-oxides will be referred as Fe-oxides in the following discussion. Reactive Mn concentrations range from 1.6 µmol g^{-1} to 4.6 µmol g^{-1}, which are nearly two orders of magnitude higher than those of Fe (oxy)hydroxides and reactive Fe-oxides. Fe and Mn show similar distribution patterns with depth (Fig. 8). Since AVS oxidizes to dithionite and oxalate extractable Fe phases during freeze-drying or exposure to air (Canfield, 1989; Morse, 1994), the obvious peak of Fe-oxides at ~900 cm depth (Fig. 8a) is partly attributed to AVS oxidation during sample storage and treatment.

5. Discussion

5.1 The role of the SMTZ in marine vivianite authigenesis

Vivianite precipitation is favored under anoxic and non-sulfidic conditions, as typically found in lacustrine sediments (Berner, 1981; Nriagu, 1972; Rothe et al., 2016). Recently, the presence of a SMTZ has been shown to play a governing role in vivianite formation, extending the importance of vivianite authigenesis to marine settings where sulfate is more readily available (Egger et al., 2015a; Hsu et al., 2014; März et al., 2008; Slomp et al., 2013). Within the SMTZ, sulfate-driven AOM consumes sulfate and methane whilst liberating sulfide and bicarbonate to the pore water. The dissolved sulfide is rapidly fixed, initially as Fe monosulfides and ultimately, under an excess of sulfide, as pyrite. Pyrite formation within the SMTZ is characterized by strong ^{34}S enrichment along with characteristic overgrowth textures (Borowski et al., 2013; Jørgensen et al., 2004; Lin et al., 2016a; Lin et al., 2016b). In addition, sulfate driven AOM enriches authigenic carbonates in ^{12}C, as they inherit their isotopic signature from ^{13}C-depleted methane (Peckmann and Thiel, 2004; Treude et al., 2005). At Site 973-4, between 600 and 900 cm depth, a pronounced increase in ^{34}S-enriched pyrite is seen in association with an excursion to low $\delta^{13}C$ values of the total inorganic carbon pool (Fig. 9). The ^{34}S enrichment in pyrite and ^{13}C depletion in total inorganic carbon indicate the position of the SMTZ, which is consistent with the estimated SMTZ depth based on pore water profiles of sulfate and methane at the adjacent sites (Fig. 2b). The lower magnetic susceptibility (Fig. 8b), because of the conversion of Fe-oxides to pyrite, provides further evidence for the location of the SMTZ around 600–900 cm depth.

Reactive Fe-oxides and Fe-rich silicates are gradually consumed within the SMTZ via reductive dissolution by sulfide and subsequent conversion to pyrite (Figs. 7b and 8a). As a consequence, any excess sulfide diffusing downwards from the SMTZ is being trapped as Fe monosulfides upon reaction with more readily available Fe-oxides at depth. This reaction zone, often referred to as the sulfidization front (S-front), is a common feature in Fe-rich marine sediments (Egger et al., 2016; Holmkvist et al., 2014; Jørgensen et al., 2004; Riedinger et al., 2017) and is recorded at Site 973-4 as a pronounced AVS peak at ~900cm depth (Fig. 9b). Besides liberating Fe, and subsequently precipitating Fe-sulfides, reductive dissolution of Fe-oxides by sulfide also releases significant amounts of Fe-oxide bound P into the pore water around the SMTZ (Egger et al., 2015a; März et al., 2008; Schulz et al., 1994; Slomp et al., 2013). This sediment-sourced PO_4 then becomes available for subsurface vivianite precipitation providing its concentration, along with that of ferrous Fe, exceeds saturation with respect to vivianite. Unfortunately, no PO_4 pore water profile is available at our site; however, the conversion of Fe-oxides to pyrite around the SMTZ and the associated release of Fe-oxide bound P to the pore water should also be recorded as relative minima in sedimentary Fe-bound P concentrations (Egger et al., 2015a, 2016). The distinct minimum of Fe-bound P around the SMTZ, and a sharp peak directly below the SMTZ, indicates that sink-switching from Fe-oxide bound P to reduced Fe-phosphates is most likely occurring at our study site (Fig. 9b).

X-ray diffraction analyses show that the blue to black aggregates found exclusively below the SMTZ are vivianite aggregates (Fig. 5a). Other Mg- or Fe-bearing phosphate minerals such as metavivianite were absent from the XRD spectra, advocating that the Fe-P-O aggregates identified by SEM-EDS and Raman are indeed vivianite (Figs. 3 and 5). The restriction of vivianite nodules to below the SMTZ strongly supports the SMTZ-catalyzed model of vivianite authigenesis resulting from inferences gleaned from the juxtaposition of lacustrine and post-glacial marine sediments (Egger et al., 2015a, 2016; Slomp et al., 2013). Furthermore, the broad peak in Fe-bound P above the SMTZ likely reflects re-adsorption of upward diffusing dissolved PO_4 to Fe-oxides present at shallower depth (Fig. 9b), as suggested previously based on observations from the Zambezi deep-sea fan (März et al., 2008).

Vivianite is reactive toward sulfide and, hence, would be readily converted to Fe-sulfide phases under H_2S-rich conditions (Berner, 1981). Therefore, when the SMTZ was shallower, vivianite was probably precipitated above where it is currently observed, and has subsequently been dissolved by the presence of sulfide. Tentative evidence for diagenetic modification of vivianite distribution is seen in the XRD spectrum. Here, XRD analysis indicates the presence of vivianite within the current SMTZ at 747 cm depth, yet handpicking failed to identify any coarse vivianite (Figs. 6–7a). Dissolution of freshly precipitated vivianite should be promoted by the downward migration of the SMTZ and increased environmental sulfide availability, producing the observed stratigraphic distribution (Fig. 7a). In the event of the SMTZ shallowing, any sub-SMTZ vivianite could therefore be preserved under the resultant H_2S-free environments.

5.2 The importance of anaerobic oxidation of methane in vivianite authigenesis

The ubiquity of vivianite aggregates below the SMTZ at Site 973-4 requires that there is a deep source of Fe^{2+}. Recent field and laboratory studies have suggested that anaerobic oxidation of methane can be coupled to the reduction of Fe-oxides (Beal

et al., 2009; Egger et al., 2015b, 2016, 2017; Riedinger et al., 2014; Sivan et al., 2011). Specifically, it has been suggested that insoluble Fe-oxides can be exploited by solitary anaerobic methanotrophic archaea (ANME) as electron acceptors, facilitating methane oxidation via extracellular electron transfer (McGlynn et al., 2015; Rotaru and Thamdrup, 2016; Scheller et al., 2016; Wegener et al., 2015). Moreover, sediment incubation experiments demonstrate that more poorly reactive Fe minerals (e.g., magnetite and hematite) are also bioavailable and, therefore, could potentially fuel Fe-AOM (Bar-Or et al., 2017). Extending these in vitro observations to natural settings suggests that bioavailable Fe-oxides, and potentially reactive Fe-rich silicates below the SMTZ may be available for bacterial Fe reduction coupled to methane oxidation. Considering the 8:1 Fe-CH_4 stoichiometry (Eq. 1; Beal et al., 2009), Fe-AOM certainly has the potential to yield significant quantities of Fe^{2+}. In general, large amounts of dissolved PO_4 are released into the pore water by sulfate-driven AOM within the SMTZ, while bacterial Fe reduction using Fe-oxides below the SMTZ triggers the release of both Fe^{2+} and PO_4 (Egger et al., 2015a). Supported by abundant Fe-oxides and Fe-silicates below the SMTZ, bacterial Fe reduction, probably driven by methane oxidation, promotes vivianite authigenesis, exchanging P originally associated with Fe-oxides to vivianite-housed P—A process referred to as sink-switching (Fig. 10). As a byproduct, Fe-AOM is known to produce alkalinity (Beal et al., 2009), which can stabilize vivianite by raising the pH values of the pore water to between 6 and 9 (Rothe et al., 2016).

Besides Fe-AOM, other potential sources of Fe^{2+} below the SMTZ include organoclastic Fe reduction (Lovley, 1997; Severmann et al., 2006) and abiotic reductive dissolution by sulfide (Canfield et al., 1992; Poulton et al., 2004). A pronounced AVS peak at ~900 cm depth constrains the depth of the sulfidization front at Site 973-4 (Fig. 9b). In similar systems, dissolved sulfide is limited below the S-front (Egger et al., 2016; Jørgensen et al., 2004; Riedinger et al., 2017). As vivianite is unstable in the presence of sulfide (Dijkstra et al., 2018a), its presence below ~920 cm depth supports the absence of appreciable amounts of dissolved sulfide. Additionally, extremely elevated concentrations of Fe^{2+} are frequently observed below the S-front (Egger et al., 2016; Holmkvist et al., 2011, 2014; Jørgensen et al., 2004; Treude et al., 2014). Given the reactivity of Fe^{2+} toward sulfide, the existence of the latter would rapidly titrate the former, forming Fe monosulfide rather than reacting with Fe-oxides (Berner, 1967). We therefore conclude that abiotic sulfide-mediated reductive dissolution of Fe-oxides is unlikely to provide significant amounts of Fe^{2+} below the SMTZ at our study site.

Although unequivocally precluding organoclastic Fe reduction below the SMTZ remains difficult, the total organic carbon content throughout core 973-4 is low and more-or-less invariant, with an average value of 0.72 ± 0.19 wt.% (Zhang et al., 2014). These relatively low concentrations of likely reworked organic matter may be insufficient for organoclastic Fe reduction (Riedinger et al., 2014). As a consequence, the importance of organoclastic Fe reduction is likely to be limited by the quality and quantity of organic matter burial below the SMTZ (Egger et al., 2017; Riedinger et al., 2014; Sivan et al., 2011).

Besides its major constituents (Fe, O and P), sedimentary vivianite aggregates are usually enriched in other minor elements, such as Mg (Burns, 1997; Dijkstra et al., 2018b; Hsu et al., 2014) or Mn (Dijkstra et al., 2018b; Egger et al., 2015a; Fagel et al., 2005; Nakano, 1992; Sapota et al., 2006). In the absence of appropriate pore water data, we rely on datasets from a proximal site that reveals high concentrations of dissolved Mg (48.7–53.0 mM) but low concentrations of dissolved Mn (0.4–5.1 µM) (Site D-5, Hu et al., 2015). These pore water concentrations are reflected in the elemental composition of Mg-rich vivianite

isolated from core 973-4 (Fig. 4). Manganese displays similar geochemical properties as Fe, yet it has been shown to be a substantially more energetically favorable electron acceptor during organic matter or methane oxidation (Beal et al., 2009). We reconcile the extremely low vivianite-housed Mn contents at Site 973-4 with the generally low sedimentary Mn-abundances (Fig. 8b) and inferred pore water Mn-availability, concluding that Mn-mediated AOM is probably of limited importance at our study site. Taken together, while we cannot completely exclude organoclastic Fe reduction as a potential source of Fe^{2+}, along with observations of others, we use the discussed stratigraphic distribution of various sedimentary mineral phases to argue that Fe-AOM is the most likely deep source of Fe^{2+} necessary to promote vivianite authigenesis observed below the SMTZ.

5.3 Quantifying the importance of vivianite authigenesis as iron and phosphorus sinks

Sequential P extractions (SEDEX; Ruttenberg, 1992), conducted by Zhang et al. (2018b), demonstrate that authigenic carbonate fluorapatite (Ca-P, Fig. 9c) accounts for up to 55% of the total P (702 µmol g^{-1}) buried at Site 973-4. Fe-bound P is generally lower than authigenic Ca–P, accounting for 27% and 13% of the total P burial above (613 µmol g^{-1}) and below the SMTZ (844 µmol g^{-1}), respectively. These results emphasize the role of Fe-bound P as an important mechanism for long-term P burial in continental margin settings (Slomp et al., 1996). Interestingly, the ratio between Fe-oxides and Fe-bound P is also apparently depth dependent; decreasing from approximately 3 at the sediment surface, to 1.8 below the SMTZ. This decrease indicates a depth-dependent change in the relative contribution of authigenic phases responsible for P sequestration. Consistent with observational and geochemical evidence for the presence of authigenic vivianite (Fig. 7a), the decrease in the Fe-oxides/Fe-bound P ratio to 1.8 approximates the stoichiometric Fe/P of vivianite (1.5), again advocating that vivianite authigenesis below the SMTZ is a potentially important process responsible for P burial at Site 973-4.

Previous studies have shown that vivianite dissolves in both the citrate-dithionite-bicarbonate (CDB; Nembrini et al., 1983) and dithionite steps (Dijkstra et al., 2014) of the sequential P- and Fe-extractions, respectively. Thus, both fractions contain P and Fe derived from vivianite (P_{viv} and Fe_{viv}) and Fe-oxides (P_{FeOx} and Fe_{FeOx}). Consequently, the total amount of P extracted during the CDB step is the sum of P_{viv} and P_{FeOx}, while the total amount of Fe extracted during the dithionite steps is the sum of Fe_{viv} and Fe_{FeOx}. Combining these measured fractions with the Fe_{FeOx}/P_{FeOx} ratio of surface sediments at our site (~3) as a measure of P binding capacity and the stoichiometric Fe/P ratio of vivianite (1.5), we can estimate the quantitative importance of vivianite burial via the approach outlined by Egger et al. (2015a). Here, adopting average concentrations of Fe-bound P (108.3 µmol g^{-1}, Fig. 9b) and Fe-oxides (196.4 µmol g^{-1}, Fig. 8a) from below the sulfidization front at Site 973-4, a set of four equations, with an equal number of unknowns can be written:

$$Fe_{FeOx} + Fe_{viv} = 196.4 \text{ µmol } g^{-1} \quad \text{(Eq.2)}$$

$$P_{FeOx} + P_{viv} = 108.3 \text{ µmol } g^{-1} \quad \text{(Eq.3)}$$

$$Fe_{FeOx} = 3P_{FeOx} \quad \text{(Eq.4)}$$

$$Fe_{viv} = 1.5P_{viv} \quad \text{(Eq.5)}$$

Simultaneously solving these equations for Fe_{viv} and P_{viv} reveals that ~129 µmol g^{-1} of the Fe extracted during the dithionite extraction, along with ~86 µmol g^{-1} of the Fe-bound P, originated from vivianite, accounting for ~79% of the total Fe-bound P below the SMTZ. Authigenic Ca-P is the major P sink (~55%) at Site 973-4, in agreement with its globally estimated importance (~50%; Ruttenberg, 2014; Ruttenberg and Berner, 1993). Vivianite, by contrast, houses approximately 10% of the sub-SMTZ P inventory. These results further suggest that only 1 to 7.3% (average and maximum, n=70) of the chemically-constrained vivianite was recovered as coarse aggregates (Fig. 7a). This discrepancy, in turn, implies that much of the authigenic vivianite fraction is either disseminated as smaller crystals (< 65 µm) or as an amorphous solid phase.

Vivianite further plays an important role in Fe cycling below the SMTZ. The sediment column at Site 973-4 can be divided at ~900 cm depth, forming two distinct geochemical zones with different Fe, P and S systematics. Thus, several additional ratios can be calculated based on the previously discussed Fe- and P-extractions (Table 1). Total reactive Fe includes Fe-oxides and their authigenic reduction products (e.g., vivianite, pyrite and Fe carbonates). Considering that total Fe abundances (725 ± 30 µmol g^{-1}) are broadly invariant below 600 cm depth (Zhang et al., 2018b), and that the maximum AVS content (9.3 mmol g^{-1}) is one order of magnitude more abundant than total Fe, either we need to reconsider the quality of the AVS measurements (Zhang et al., 2014), or much of the quantified AVS (mainly H_2S + FeS) reflects dissolved sulfide, rather than Fe sulfides (Fig. 9b). Given the difficulties in deconvolving the relative importance of FeS and dissolved sulfide, coupled with the likely restriction of FeS to the sulfidization front at ~900 cm depth (Fig. 9b), FeS is precluded from further discussion.

Moving forward, however, this approach reveals that 52% of Fe-oxides were likely reduced to pyrite within the SMTZ, whereas 41% were converted to vivianite below the SMTZ. While vivianite may represent a major component of total P inventory below the SMTZ in coastal settings (40–50%; Egger et al., 2015a), its importance as an Fe sink is muted, representing only a small fraction of the of total reactive Fe budget in the Baltic Sea sediments (~6.4%; Rooze et al., 2016). At Site 973-4, however, vivianite accounts for almost half of the reactive Fe burial below the SMTZ, arguing that vivianite may represent an important Fe burial phase in methane-rich deep-sea sediments. Considering the concentrations of total Fe are broadly constant below 600 cm depth at Site 973-4, Fe reduction contributes similar amounts of Fe(II) (~34% and ~32% of total Fe) below and within the SMTZ providing Fe(II) phases here are authigenic. Hence, besides abiotic reductive dissolution of Fe-oxides within the SMTZ, Fe cycling is strongly affected by Fe reduction at depth. Based on the discussion above, we argue that Fe-AOM is a likely source of reduced Fe, which may sequester around 34% of total Fe as reduced burial phase below the SMTZ. Accordingly, bacterial Fe reduction coupled to AOM may play an important role for Fe and P cycling at depth.

While the detailed mineralogical work necessary to confirm the spatial importance of vivianite authigenesis in open marine sediments awaits, at least at Site 973-4, vivianite authigenesis proceeds below the SMTZ, driven apparently by deep Fe reduction which, in the absence of free sulfide, supplies copious quantities of pore water Fe^{2+} and PO_4. Therefore, it follows that substantial burial of vivianite below the SMTZ associated with Fe reduction will have significantly altered the sedimentary record. The absence of sulfide at depth below the SMTZ indicates that vivianite associated with paleo-SMTZs may be preserved over geological timescales in sediments providing the SMTZ does not penetrate deeper into the sediment column, thus there may be deeper layers of vivianite preserved within the 3–4 km thick sediment package preserved in the Taixinan

Basin (McDonnell et al., 2000). Consequently, extra caution is warranted when using sedimentary P distributions of methane-rich sediments to reconstruct past ocean primary productivity and P burial pathways (Dijkstra et al., 2018a).

5.4 Vivianite as a possible proxy for Fe-AOM

If Fe-AOM represents the main source of Fe^{2+} below the SMTZ, the presence of vivianite could also potentially serve as a proxy for Fe-AOM in the sedimentary record. Hence, our findings may have potential implications for elemental cycling and redox conditions throughout the Earth's history (Beal et al., 2009; Riedinger et al., 2014), particularly prior to the first accumulation of oxygen 2.3 billion-years ago during the so-called Great Oxidation Event (GOE; Luo et al., 2016; Lyons et al., 2014). Prior to the GOE, the Earth system was drastically different, with an oxygen poor atmosphere curtailing oxidative weathering and stabilizing an iron-rich, sulfate-poor ocean (Canfield et al., 2000; Poulton and Canfield, 2011). Within present-day oceans, sulfate-driven AOM is known to almost entirely consume methane, serving as an efficient sedimentary methane filter, and preventing this potent greenhouse gas from reaching the atmosphere (Egger et al., 2018; Knittel and Boetius, 2009). In the low sulfate pre-GOE oceans, however, sulfate scarcity may have limited methane oxidation, potentially allowing it to accumulate in the atmosphere (Habicht et al., 2002; Izon et al., 2015, 2017; Kasting et al., 2001). Against this sulfate-lean backdrop, the prevalence of Fe oxide-rich deposits known as banded iron formations (BIFs) dating from the Archean and early Paleoproterozoic (Klein, 2005; Konhauser et al., 2002), are testament to the ubiquity of Fe within the Earth's early oceans. It is possible, therefore, that Fe-AOM was a much more important process within Earth's oxygen deficient early oceans relative to their contemporary counterparts. If true, the interplay between Fe and methane, especially in the prelude of the GOE (e.g., Izon et al., 2017), could have modulated the methane efflux from the ocean to the atmosphere (Riedinger et al., 2014). Thus, a better understanding of vivianite authigenesis is fundamental to test long-standing hypotheses linking climate, atmospheric chemistry and the evolution of the biosphere.

6 Conclusions

Combining bulk geochemical extractions with microscopic and spectroscopic analyses of handpicked mineral aggregates, we show that vivianite formation occurs within the iron- and methane-rich sediments from the Taixinan Basin, South China Sea. The identified vivianite aggregates are enriched in magnesium but are depleted in manganese, reflecting their growth environment. We argue that as the source of Fe^{2+} for vivianite authigenesis, Fe reduction below the SMTZ was probably driven by Fe-mediated anaerobic oxidation of methane, which has broad implications for Fe and P cycling at depth. Importantly, vivianite authigenesis appears to be restricted to sediments below the SMTZ, where it accounts for ~79% of the Fe-bound P and ~10% of the total sub-SMTZ P burial, respectively. Notably, we calculate that vivianite may constitute almost half of the total reactive Fe burial below the SMTZ at Site 973-4. Geochemical conditions that characterize site 973-4 are not uncommon and typify continental margin environments (Kasten et al., 1998; März et al., 2008; Riedinger et al., 2014). Thus, vivianite may be an important burial phase for P and Fe below the SMTZ in present-day marine systems. We further speculate that

authigenic vivianite might serve as a proxy for Fe-mediated AOM allowing its importance to be evaluated throughout Earth's history.

Acknowledgements

Qi Lin is acknowledged for providing insight into the study area; whereas formative discussions with Bo Barker Jørgensen, Samantha Joye and Alexandra V. Turchyn helped shape the preparation of this manuscript. We recognize technical assistance from Xiaoping Liao, Wanjun Lu, Chao Li, Caixiang Zhang and Zihu Zhang at CUG, Wuhan. Daidai Wu, Jie Zhang and Wenjia Ou graciously shared data. The Guangzhou Marine Geological Survey, along with the crew and scientists on board R/V *Ocean VI* are acknowledged for sampling and logistical support. This research was funded by State Key R&D Project of China (Grant 2016YFA0601102), National Natural Science Foundation of China (Grants 41772091 and 41472085) and National Special Program of Gas Hydrate in China. JL acknowledges financial support via the international exchange program at the School of Earth Sciences, CUG. GI gratefully recognizes support from the Simons Foundation, who funded his contribution under the auspices of the collaboration on the origin of life. Partial travel support from CUG (Beijing and Wuhan) initiated GI's interest in vivianite.

References

Algeo, T. J., and Ingall, E.: Sedimentary Corg:P ratios, paleocean ventilation, and Phanerozoic atmospheric pO2, Palaeogeogr., Palaeoclimatol., Palaeoecol., 256, 130-155, doi:10.1016/j.palaeo.2007.02.029, 2007.

Amonette, J. E., and Templeton, J. C.: Improvements to the quantitative assay of nonrefractory minerals for Fe (II) and total Fe using 1, 10-phenanthroline, Clays Clay Miner., 46, 51-62, doi:10.1346/CCMN.1998.0460106, 1998.

Amos, R., Bekins, B., Cozzarelli, I., Voytek, M., Kirshtein, J., Jones, E., and Blowes, D.: Evidence for iron-mediated anaerobic methane oxidation in a crude oil-contaminated aquifer, Geobiology, 10, 506-517, doi:10.1111/j.1472-4669.2012.00341.x, 2012.

Bar-Or, I., Elvert, M., Eckert, W., Kushmaro, A., Vigderovich, H., Zhu, Q., Ben-Dov, E., and Sivan, O.: Iron-Coupled Anaerobic Oxidation of Methane Performed by a Mixed Bacterial-Archaeal Community Based on Poorly Reactive Minerals, Environ. Sci. Technol., 51, 12293-12301, doi:10.1021/acs.est.7b03126, 2017.

Beal, E. J., House, C. H., and Orphan, V. J.: Manganese-and iron-dependent marine methane oxidation, Science, 325, 184-187, doi:10.1126/science.1169984, 2009.

Berner, R. A.: Thermodynamic stability of sedimentary iron sulfides, Am. J. Sci., 265, 773-785, doi:10.2475/ajs.265.9.773, 1967.

Berner, R. A.: A new geochemical classification of sedimentary environments, J. Sediment. Res., 51, 359-365, doi:10.1306/212F7C7F-2B24-11D7-8648000102C1865D, 1981.

Borowski, W. S., Rodriguez, N. M., Paull, C. K., and Ussler III, W.: Are 34S-enriched authigenic sulfide minerals a proxy for elevated methane flux and gas hydrates in the geologic record?, Mar. Pet. Geol., 43, 381-395, doi:10.1016/j.marpetgeo.2012.12.009, 2013.

Burns, S.: Early diagenesis in Amazon fan sediments, in: Proc. ODP Sci. Results, edited by: Flood, R. D., Piper, D. J. W., Klaus, A., and Peterson, L. C., Texas, USA, 497-504, 1997.

Canfield, D. E.: Reactive iron in marine sediments, Geochim. Cosmochim. Ac., 53, 619-632, doi:10.1016/0016-7037(89)90005-7, 1989.

Canfield, D. E., Raiswell, R., and Bottrell, S. H.: The reactivity of sedimentary iron minerals toward sulfide, Am. J. Sci., 292, 659-683, doi:10.2475/ajs.292.9.659, 1992.

Canfield, D. E., Habicht, K. S., and Thamdrup, B.: The Archean Sulfur Cycle and the Early History of Atmospheric Oxygen, Science, 288, 658-661, doi:10.1126/science.288.5466.658, 2000.

Crowe, S., Katsev, S., Leslie, K., Sturm, A., Magen, C., Nomosatryo, S., Pack, M., Kessler, J., Reeburgh, W., and Roberts, J.: The methane cycle in ferruginous Lake Matano, Geobiology, 9, 61-78, doi:10.1111/j.1472-4669.2010.00257.x, 2011.

Delaney, M.: Phosphorus accumulation in marine sediments and the oceanic phosphorus cycle, Global Biogeochem. Cycles, 12, 563-572, doi:10.1029/98GB02263, 1998.

Dijkstra, N., Kraal, P., Kuypers, M. M., Schnetger, B., and Slomp, C. P.: Are iron-phosphate minerals a sink for phosphorus in anoxic Black Sea sediments?, PloS one, 9, e101139, doi:10.1371/journal.pone.0101139, 2014.

Dijkstra, N., Slomp, C. P., and Behrends, T.: Vivianite is a key sink for phosphorus in sediments of the Landsort Deep, an intermittently anoxic deep basin in the Baltic Sea, Chem. Geol., 438, 58-72, doi:10.1016/j.chemgeo.2016.05.025, 2016.

Dijkstra, N., Hagens, M., Egger, M., and Slomp, C. P.: Post-depositional formation of vivianite-type minerals alters sediment phosphorus records, Biogeosciences, 15, 861-883, doi:10.5194/bg-2017-295, 2018a.

Dijkstra, N., Krupinski, N. B. Q., Yamane, M., Obrochta, S. P., Miyairi, Y., Yokoyama, Y., and Slomp, C. P.: Holocene refreshening and reoxygenation of a Bothnian Sea estuary led to enhanced phosphorus burial, Estuar. Coast., 41, 139-157, doi:10.1007/s12237-017-0262-x, 2018b.

Egger, M., Jilbert, T., Behrends, T., Rivard, C., and Slomp, C. P.: Vivianite is a major sink for phosphorus in methanogenic coastal surface sediments, Geochim. Cosmochim. Ac., 169, 217-235, doi:10.1016/j.gca.2015.09.012, 2015a.

Egger, M., Rasigraf, O., Sapart, C. l. J., Jilbert, T., Jetten, M. S., Röckmann, T., van der Veen, C., Bândă, N., Kartal, B., and Ettwig, K. F.: Iron-mediated anaerobic oxidation of methane in brackish coastal sediments, Environ. Sci. Technol., 49, 277-283, doi:10.1021/es503663z, 2015b.

Egger, M., Kraal, P., Jilbert, T., Sulu-Gambari, F., Sapart, C. J., Röckmann, T., and Slomp, C. P.: Anaerobic oxidation of methane alters sediment records of sulfur, iron and phosphorus in the Black Sea, Biogeosciences, 13, 5333-5355, doi:10.5194/bg-13-5333-2016, 2016.

Egger, M., Hagens, M., Sapart, C. J., Dijkstra, N., van Helmond, N. A., Mogollón, J. M., Risgaard-Petersen, N., van der Veen, C., Kasten, S., and Riedinger, N.: Iron oxide reduction in methane-rich deep Baltic Sea sediments, Geochim. Cosmochim. Ac., 207, 256-276, doi:10.1016/j.gca.2017.03.019, 2017.

Egger, M., Riedinger, N., Mogollón, J. M., and Jørgensen, B. B.: Global diffusive fluxes of methane in marine sediments, Nat. Geosci., doi:10.1038/s41561-018-0122-8, 2018.

Ettwig, K. F., Zhu, B., Speth, D., Keltjens, J. T., Jetten, M. S., and Kartal, B.: Archaea catalyze iron-dependent anaerobic oxidation of methane, P. Natl. Acad. Sci. USA, 113, 12792-12796, doi:10.1073/pnas.1609534113, 2016.

Fagel, N., Alleman, L., Granina, L., Hatert, F., Thamo-Bozso, E., Cloots, R., and André, L.: Vivianite formation and distribution in Lake Baikal sediments, Global Planet. Change, 46, 315-336, doi:10.1016/j.gloplacha.2004.09.022, 2005.

Feng, D., and Chen, D.: Authigenic carbonates from an active cold seep of the northern South China Sea: new insights into fluid sources and past seepage activity, Deep-Sea Res. Pt. II, 122, 74-83, doi:10.1016/j.dsr2.2015.02.003, 2015.

Feng, D., Cheng, M., Kiel, S., Qiu, J.-W., Yang, Q., Zhou, H., Peng, Y., and Chen, D.: Using Bathymodiolus tissue stable carbon, nitrogen and sulfur isotopes to infer biogeochemical process at a cold seep in the South China Sea, Deep-Sea Res. Pt. I, 104, 52-59, doi:10.1016/j.dsr.2015.06.011, 2015.

Grizelj, A., Bakrač, K., Horvat, M., Avanić, R., and Hećimović, I.: Occurrence of vivianite in alluvial Quaternary sediments in the area of Sesvete (Zagreb, Croatia), Geologia Croatica, 70, 41-52, doi:10.4154/gc.2017.01, 2017.

Habicht, K. S., Gade, M., Thamdrup, B., Berg, P., and Canfield, D. E.: Calibration of Sulfate Levels in the Archean Ocean, Science, 298, 2372-2374, doi:10.1126/science.1078265, 2002.

Han, X., Suess, E., Huang, Y., Wu, N., Bohrmann, G., Su, X., Eisenhauer, A., Rehder, G., and Fang, Y.: Jiulong methane reef: microbial mediation of seep carbonates in the South China Sea, Mar. Geol., 249, 243-256, doi:10.1016/j.margeo.2007.11.012, 2008.

Holmkvist, L., Ferdelman, T. G., and Jørgensen, B. B.: A cryptic sulfur cycle driven by iron in the methane zone of marine sediment (Aarhus Bay, Denmark), Geochim. Cosmochim. Ac., 75, 3581-3599, doi:10.1016/j.gca.2011.03.033, 2011.

Holmkvist, L., Kamyshny Jr, A., Bruechert, V., Ferdelman, T. G., and Jørgensen, B. B.: Sulfidization of lacustrine glacial clay upon Holocene marine transgression (Arkona Basin, Baltic Sea), Geochim. Cosmochim. Ac., 142, 75-94, doi:10.1016/j.gca.2014.07.030, 2014.

Hsu, H.-H., Liu, C.-S., Morita, S., Tu, S.-L., Lin, S., Machiyama, H., Azuma, W., Ku, C.-Y., and Chen, S.-C.: Seismic imaging of the Formosa Ridge cold seep site offshore of southwestern Taiwan, Mar. Geophys. Res., 1-13, doi:10.1007/s11001-017-9339-y, 2017.

Hsu, T.-W., Jiang, W.-T., and Wang, Y.: Authigenesis of vivianite as influenced by methane-induced sulfidization in cold-seep sediments off southwestern Taiwan, J. Asian Earth Sci., 89, 88-97, doi:10.1016/j.jseaes.2014.03.027, 2014.

Hu, Y., Feng, D., Liang, Q., Xia, Z., Chen, L., and Chen, D.: Impact of anaerobic oxidation of methane on the geochemical cycle of redox-sensitive elements at cold-seep sites of the northern South China Sea, Deep-Sea Res. Pt. II, 122, 84-94, doi:10.1016/j.dsr2.2015.06.012, 2015.

Izon, G., Zerkle, A. L., Zhelezinskaia, I., Farquhar, J., Newton, R. J., Poulton, S. W., Eigenbrode, J. L., and Claire, M. W.: Multiple oscillations in Neoarchaean atmospheric chemistry, Earth. Planet. Sci. Lett., 431, 264-273, doi:10.1016/j.epsl.2015.09.018, 2015.

Izon, G., Zerkle, A. L., Williford, K. H., Farquhar, J., Poulton, S. W., and Claire, M. W.: Biological regulation of atmospheric chemistry en route to planetary oxygenation, P. Natl. Acad. Sci. USA, 114, E2571-E2579, doi:10.1073/pnas.1618798114, 2017.

Jensen, H. S., Mortensen, P. B., Andersen, F., Rasmusse, E., and Jensen, A.: Phosphorus cycling in a coastal marine sediment, Aarhus Bay, Denmark, Limnol. Oceanogr., 40, 908-917, doi:10.4319/lo.1995.40.5.0908, 1995.

Jørgensen, B. B., Böttcher, M. E., Lüschen, H., Neretin, L. N., and Volkov, I. I.: Anaerobic methane oxidation and a deep H2S sink generate isotopically heavy sulfides in Black Sea sediments, Geochim. Cosmochim. Ac., 68, 2095-2118, doi:10.1016/j.gca.2003.07.017, 2004.

Kagan, M. R., and McCreery, R. L.: Reduction of fluorescence interference in Raman spectroscopy via analyte adsorption on graphitic carbon, Anal. Chem., 66, 4159-4165, doi:10.1021/ac00095a008, 1994.

Kasten, S., Freudenthal, T., Gingele, F. X., and Schulz, H. D.: Simultaneous formation of iron-rich layers at different redox boundaries in sediments of the Amazon deep-sea fan, Geochim. Cosmochim. Ac., 62, 2253-2264, doi:10.1016/S0016-7037(98)00093-3, 1998.

Kasting, J. F., Pavlov, A. A., and Siefert, J. L.: A Coupled Ecosystem-Climate Model for Predicting the Methane Concentration in the Archean Atmosphere, Origins Life Evol. Biosphere, 31, 271-285, doi:10.1023/a:1010600401718, 2001.

Kennett, J. P., Cannariato, K. G., Hendy, I. L., and Behl, R. J.: Methane Hydrates in Quaternary Climate Change: The Clathrate Gun Hypothesis, American Geophysical Union, Washington, DC, USA, 2003.

Klein, C.: Some Precambrian banded iron-formations (BIFs) from around the world: Their age, geologic setting, mineralogy, metamorphism, geochemistry, and origins, Am. Mineral., 90, 1473-1499, doi:10.2138/am.2005.1871, 2005.

Knittel, K., and Boetius, A.: Anaerobic oxidation of methane: progress with an unknown process, Annu. Rev. Microbiol., 63, 311-334, doi:10.1146/annurev.micro.61.080706.093130, 2009.

Konhauser, K. O., Hamade, T., Raiswell, R., Morris, R. C., Ferris, F. G., Southam, G., and Canfield, D. E.: Could bacteria have formed the Precambrian banded iron formations?, Geology, 30, 1079-1082, doi:10.1130/0091-7613(2002)030<1079:CBHFTP>2.0.CO;2, 2002.

Lin, Q., Wang, J., Fu, S., Lu, H., Bu, Q., Lin, R., and Sun, F.: Elemental sulfur in northern South China Sea sediments and its significance, Sci. China Earth Sci., 58, 2271-2278, doi:10.1007/s11430-015-5182-7, 2015.

Lin, Q., Wang, J., Algeo, T. J., Sun, F., and Lin, R.: Enhanced framboidal pyrite formation related to anaerobic oxidation of methane in the sulfate-methane transition zone of the northern South China Sea, Mar. Geol., 379, 100-108, doi:10.1016/j.margeo.2016.05.016, 2016a.

Lin, R., Wang, J., Su, P., Lin, Q., Sun, F., and Yang, J.: Characteristics of magnetic susceptibility of cored sediments and their implications for the potential methane events in northern South China Sea, Acta Sedimentologica Sinica, 35, 290-298, doi:10.14027/j.cnki.cjxb.2017.02.008, 2017a.

Lin, Z., Sun, X., Peckmann, J., Lu, Y., Xu, L., Strauss, H., Zhou, H., Gong, J., Lu, H., and Teichert, B. M. A.: How sulfate-driven anaerobic oxidation of methane affects the sulfur isotopic composition of pyrite: A SIMS study from the South China Sea, Chem. Geol., 440, 26-41, doi:10.1016/j.chemgeo.2016.07.007, 2016b.

Lin, Z., Sun, X., Strauss, H., Lu, Y., Gong, J., Xu, L., Lu, H., Teichert, B. M., and Peckmann, J.: Multiple sulfur isotope constraints on sulfate-driven anaerobic oxidation of methane: Evidence from authigenic pyrite in seepage areas of the South China Sea, Geochim. Cosmochim. Ac., 211, 153-173, doi:10.1016/j.gca.2017.05.015, 2017b.

Liu, C.-S., Huang, I. L., and Teng, L. S.: Structural features off southwestern Taiwan, Mar. Geol., 137, 305-319, doi:10.1016/S0025-3227(96)00093-X, 1997.

Lovley, D. R.: Microbial Fe (III) reduction in subsurface environments, FEMS Microbiol. Rev., 20, 305-313, doi:10.1111/j.1574-6976.1997.tb00316.x, 1997.

Lu, H., Liu, J., Chen, F., Cheng, S., and Liao, Z.: Shallow sulfate-methane interface in northeastern South China Sea: An indicator of strong methane seepage on seafloor, Mar Geol Quat Geol, 32, 93-98, doi:10.3724/SP.J.1140.2012.01093, 2012.

Luo, G., Ono, S., Beukes, N. J., Wang, D. T., Xie, S., and Summons, R. E.: Rapid oxygenation of Earth's atmosphere 2.33 billion years ago, Science Advances, 2, doi:10.1126/sciadv.1600134, 2016.

Lyons, T. W., Reinhard, C. T., and Planavsky, N. J.: The rise of oxygen in Earth's early ocean and atmosphere, Nature, 506, 307, doi:10.1038/nature13068, 2014.

März, C., Hoffmann, J., Bleil, U., De Lange, G., and Kasten, S.: Diagenetic changes of magnetic and geochemical signals by anaerobic methane oxidation in sediments of the Zambezi deep-sea fan (SW Indian Ocean), Mar. Geol., 255, 118-130, doi:10.1016/j.margeo.2008.05.013, 2008.

Maslin, M., Owen, M., Day, S., and Long, D.: Linking continental-slope failures and climate change: Testing the clathrate gun hypothesis, Geology, 32, 53-56, doi:10.1130/G20114.1, 2004.

McDonnell, S., Max, M., Cherkis, N. e. a., and Czarnecki, M.: Tectono-sedimentary controls on the likelihood of gas hydrate occurrence near Taiwan, Mar. Pet. Geol., 17, 929-936, doi:10.1016/S0264-8172(00)00023-4, 2000.

McGlynn, S. E., Chadwick, G. L., Kempes, C. P., and Orphan, V. J.: Single cell activity reveals direct electron transfer in methanotrophic consortia, Nature, 526, 531, doi:10.1038/nature15512, 2015.

Morse, J. W.: Interactions of trace metals with authigenic sulfide minerals: implications for their bioavailability, Mar. Chem., 46, 1-6, doi:10.1016/0304-4203(94)90040-X, 1994.

Nakano, S.: Manganoan vivianite in the bottom sediments of Lake Biwa, Japan, Mineralogical Journal, 16, 96-107, doi:10.2465/minerj.16.96, 1992.

Nembrini, G., Capobianco, J., Viel, M., and Williams, A.: A Mössbauer and chemical study of the formation of vivianite in sediments of Lago Maggiore (Italy), Geochim. Cosmochim. Ac., 47, 1459-1464, doi:10.1016/0016-7037(83)90304-6, 1983.

Norði, K. à., Thamdrup, B., and Schubert, C. J.: Anaerobic oxidation of methane in an iron-rich Danish freshwater lake sediment, Limnol. Oceanogr., 58, 546-554, doi:10.4319/lo.2013.58.2.0546, 2013.

Nriagu, J. O.: Stability of vivianite and ion-pair formation in the system Fe3(PO4)2-H3PO4-H2O, Geochim. Cosmochim. Ac., 36, 459-470, doi:10.1016/0016-7037(72)90035-X, 1972.

Ou, W.: Sedimentary organic geochemistry research of source rocks of the potential gas hydrate-bearing areas in the northern South China Sea, Ph.D. thesis, Xiamen University, China, 2013.

Peckmann, J., and Thiel, V.: Carbon cycling at ancient methane–seeps, Chem. Geol., 205, 443-467, doi:10.1016/j.chemgeo.2003.12.025, 2004.

Piriou, B., and Poullen, J.: Raman study of vivianite, J. Raman Spectrosc., 15, 343-346, doi:10.1002/jrs.1250150510, 1984.

Porrenga, D. H.: Glauconite and chamosite as depth indicators in the marine environment, Mar. Geol., 5, 495-501, doi:10.1016/0025-3227(67)90056-4, 1967.

Poulton, S. W., Krom, M. D., and Raiswell, R.: A revised scheme for the reactivity of iron (oxyhydr) oxide minerals towards dissolved sulfide, Geochim. Cosmochim. Ac., 68, 3703-3715, doi:10.1016/j.gca.2004.03.012, 2004.

Poulton, S. W., and Canfield, D. E.: Development of a sequential extraction procedure for iron: implications for iron partitioning in continentally derived particulates, Chem. Geol., 214, 209-221, doi:10.1016/j.chemgeo.2004.09.003, 2005.

Poulton, S. W., and Canfield, D. E.: Ferruginous Conditions: A Dominant Feature of the Ocean through Earth's History, Elements, 7, 107-112, doi:10.2113/gselements.7.2.107, 2011.

Raiswell, R., Canfield, D., and Berner, R.: A comparison of iron extraction methods for the determination of degree of pyritisation and the recognition of iron-limited pyrite formation, Chem. Geol., 111, 101-110, doi:10.1016/0009-2541(94)90084-1, 1994.

Reed, D. C., Gustafsson, B. G., and Slomp, C. P.: Shelf-to-basin iron shuttling enhances vivianite formation in deep Baltic Sea sediments, Earth. Planet. Sci. Lett., 434, 241-251, doi:10.1016/j.epsl.2015.11.033, 2016.

Riedinger, N., Formolo, M. J., Lyons, T. W., Henkel, S., Beck, A., and Kasten, S.: An inorganic geochemical argument for coupled anaerobic oxidation of methane and iron reduction in marine sediments, Geobiology, 12, 172-181, doi:10.1111/gbi.12077, 2014.

Riedinger, N., Brunner, B., Krastel, S., Arnold, G. L., Wehrmann, L. M., Formolo, M. J., Beck, A., Bates, S. M., Henkel, S., and Kasten, S.: Sulfur cycling in an iron oxide-dominated, dynamic marine depositional system: The Argentine continental margin, Front. Earth Sci., 5, 33, doi:10.3389/feart.2017.00033, 2017.

Rooze, J., Egger, M., Tsandev, I., and Slomp, C. P.: Iron-dependent anaerobic oxidation of methane in coastal surface sediments: Potential controls and impact, Limnol. Oceanogr., 61, doi:10.1002/lno.10275, 2016.

Rotaru, A.-E., and Thamdrup, B.: A new diet for methane oxidizers, Science, 351, 658-658, doi:10.1126/science.aaf0741, 2016.

Rothe, M., Eder, M., Kleeberg, A., and Hupfer, M.: Evidence for vivianite formation and its contribution to long-term phosphorus retention in a recent lake sediment: a novel analytical approach, Biogeosciences, 5169, doi:10.5194/bg-11-5169-2014, 2014.

Rothe, M., Kleeberg, A., Grüneberg, B., Friese, K., Pérez-Mayo, M., and Hupfer, M.: Sedimentary sulphur: iron ratio indicates vivianite occurrence: a study from two contrasting freshwater systems, Plos one, 10, e0143737, doi:10.1371/journal.pone.0143737, 2015.

Rothe, M., Kleeberg, A., and Hupfer, M.: The occurrence, identification and environmental relevance of vivianite in waterlogged soils and aquatic sediments, Earth-Sci. Rev., 158, 51-64, doi:10.1016/j.earscirev.2016.04.008, 2016.

Ruttenberg, K. C.: Development of a sequential extraction method for different forms of phosphorus in marine sediments, Limnol. Oceanogr., 37, 1460-1482, doi:10.4319/lo.1992.37.7.1460, 1992.

Ruttenberg, K. C., and Berner, R. A.: Authigenic apatite formation and burial in sediments from non-upwelling, continental margin environments, Geochim. Cosmochim. Ac., 57, 991-1007, doi:10.1016/0016-7037(93)90035-U, 1993.

Ruttenberg, K. C.: The Global Phosphorus Cycle, in: Treatise on Geochemistry (Second Edition), edited by: Turekian, K. K., Elsevier, Oxford, 499-558, 2014.

Sapota, T., Aldahan, A., and Al-Aasm, I. S.: Sedimentary facies and climate control on formation of vivianite and siderite microconcretions in sediments of Lake Baikal, Siberia, J. Paleolimnol., 36, 245-257, doi:10.1007/s10933-006-9005-x, 2006.

Scheller, S., Yu, H., Chadwick, G. L., McGlynn, S. E., and Orphan, V. J.: Artificial electron acceptors decouple archaeal methane oxidation from sulfate reduction, Science, 351, 703-707, doi:10.1126/science.aad7154, 2016.

Schulz, H. D., Dahmke, A., Schinzel, U., Wallmann, K., and Zabel, M.: Early diagenetic processes, fluxes, and reaction rates in sediments of the South Atlantic, Geochim. Cosmochim. Ac., 58, 2041-2060, doi:10.1016/0016-7037(94)90284-4, 1994.

Segarra, K. E., Comerford, C., Slaughter, J., and Joye, S. B.: Impact of electron acceptor availability on the anaerobic oxidation of methane in coastal freshwater and brackish wetland sediments, Geochim. Cosmochim. Ac., 115, 15-30, doi:10.1016/j.gca.2013.03.029, 2013.

Severmann, S., Johnson, C. M., Beard, B. L., and McManus, J.: The effect of early diagenesis on the Fe isotope compositions of porewaters and authigenic minerals in continental margin sediments, Geochim. Cosmochim. Ac., 70, doi:10.1016/j.gca.2006.01.007, 2006.

Sha, Z., Liang, J., Zhang, G., Yang, S., Lu, J., Zhang, Z., McConnell, D. R., and Humphrey, G.: A seepage gas hydrate system in northern South China Sea: Seismic and well log interpretations, Mar. Geol., 366, 69-78, doi:10.1016/j.margeo.2015.04.006, 2015.

Shi, C., Lei, H., Zhao, J., Zhang, J., and Han, C.: Vertical microbial community structure characteristics of sediment in gas hydrate potential area of northern South China Sea Jiulong Methane Reef, Acta Sedimentol Sinica, 32, 1072-1082, 2014.

Sivan, O., Adler, M., Pearson, A., Gelman, F., Bar-Or, I., John, S. G., and Eckert, W.: Geochemical evidence for iron-mediated anaerobic oxidation of methane, Limnol. Oceanogr., 56, 1536-1544, doi:10.4319/lo.2011.56.4.1536, 2011.

Slomp, C. P., Epping, E. H., Helder, W., and Raaphorst, W. V.: A key role for iron-bound phosphorus in authigenic apatite formation in North Atlantic continental platform sediments, J. Mar. Res., 54, 1179-1205, doi:10.1357/0022240963213745, 1996.

Slomp, C. P., Mort, H. P., Jilbert, T., Reed, D. C., Gustafsson, B. G., and Wolthers, M.: Coupled dynamics of iron and phosphorus in sediments of an oligotrophic coastal basin and the impact of anaerobic oxidation of methane, PloS one, 8, e62386, doi:10.1371/journal.pone.0062386, 2013.

Suess, E., Huang, Y., Wu, N., Han, X., and Su, X.: South China Sea continental margin: Geological methane budget and environmental effects of methane emissions and gas hydrates, RV SONNE Cruise Report, Leibniz Institute of Marine Sciences, Kiel, Germany, 1-154, 2005.

Sundby, B., Gobeil, C., Silverberg, N., and Alfonso, M.: The phosphorus cycle in coastal marine sediments, Limnol. Oceanogr., 37, 1129-1145, doi:10.4319/lo.1992.37.6.1129, 1992.

Tenzer, R., and Gladkikh, V.: Assessment of density variations of marine sediments with ocean and sediment depths, The Sci. World J., 2014, doi:10.1155/2014/823296, 2014.

Treude, T., Niggemann, J., Kallmeyer, J., Wintersteller, P., Schubert, C. J., Boetius, A., and Jørgensen, B. B.: Anaerobic oxidation of methane and sulfate reduction along the Chilean continental margin, Geochim. Cosmochim. Ac., 69, 2767-2779, doi:10.1016/j.gca.2005.01.002, 2005.

Treude, T., Krause, S., Maltby, J., Dale, A. W., Coffin, R., and Hamdan, L. J.: Sulfate reduction and methane oxidation activity below the sulfate-methane transition zone in Alaskan Beaufort Sea continental margin sediments: Implications for deep sulfur cycling, Geochim. Cosmochim. Ac., 144, 217-237, doi:10.1016/j.gca.2014.08.018, 2014.

Wankel, S. D., Adams, M. M., Johnston, D. T., Hansel, C. M., Joye, S. B., and Girguis, P. R.: Anaerobic methane oxidation in metalliferous hydrothermal sediments: influence on carbon flux and decoupling from sulfate reduction, Environ. Microbiol., 14, 2726-2740, doi:10.1111/j.1462-2920.2012.02825.x, 2012.

Wegener, G., Krukenberg, V., Riedel, D., Tegetmeyer, H. E., and Boetius, A.: Intercellular wiring enables electron transfer between methanotrophic archaea and bacteria, Nature, 526, 587, doi:10.1038/nature15733, 2015.

Yan, Z., Joshi, P., Gorski, C. A., and Ferry, J. G.: A biochemical framework for anaerobic oxidation of methane driven by Fe (III)-dependent respiration, Nat. commun., 9, doi:10.1038/s41467-018-04097-9, 2018.

Ye, H., Yang, T., Zhu, G., Jiang, S., and Wu, L.: Pore water geochemistry in shallow sediments from the northeastern continental slope of the South China Sea, Mar. Pet. Geol., 75, 68-82, doi:10.1016/j.marpetgeo.2016.03.010, 2016.

Zhang, B., Wu, D., and Wu, N.: Characteristics of sedimentary geochemistry and their responses to cold-seep activities in Dongsha, the northern South China Sea, Marine Geology Frontiers, 31, 14-27, 2015a.

Zhang, B., Pan, M., Wu, D., and Wu, N.: Distribution and isotopic composition of foraminifera at cold-seep Site 973-4 in the Dongsha area, northeastern South China Sea, J. Asian Earth Sci., doi:10.1016/j.jseaes.2018.05.007, 2018a.

Zhang, G., Liang, J., Lu, J. a., Yang, S., Zhang, M., Holland, M., Schultheiss, P., Su, X., Sha, Z., and Xu, H.: Geological features, controlling factors and potential prospects of the gas hydrate occurrence in the east part of the Pearl River Mouth Basin, South China Sea, Mar. Pet. Geol., 67, 356-367, doi:10.1016/j.marpetgeo.2015.05.021, 2015b.

Zhang, J., Lei, H., Ou, W., Yang, Y., Gong, C., and Shi, C.: Research of the sulfate-methane transition zone (SMTZ) in sediments of 973-4 column in continental slope of northern South China Sea, Natural Gas Geoscience, 25, 1811-1820, doi:10.11764/j.issn.1672-1926.2014.11.1811, 2014.

Zhang, J., Lei, H., Yang, M., Chen, Y., Kong, Y., and Lu, Y.: The Interactions of P-S-Fe in sediment from the continental slope of northern South China Sea and their implication for the sulfate – methane transition zone, Earth Sci. Front., 25, 285-293, doi:10.13745/j.esf.sf.2018.2.2, 2018b.

Zhong, G., Cartigny, M. J., Kuang, Z., and Wang, L.: Cyclic steps along the South Taiwan Shoal and West Penghu submarine canyons on the northeastern continental slope of the South China Sea, GSA Bulletin, 127, 804-824, doi:10.1130/B31003.1, 2015.

Zhuang, C., Chen, F., Cheng, S., Lu, H., Zhou, Y., and Liu, G.: Stable isotopic characteristics and their influencing factors of benthic foraminifera in the prospective gas hydrate area from the northern South China Sea since the last glacial, Quaternary Sciences, 35, 422-432, doi:10.11928/j.issn.1001-7410.2015.02.17, 2015.

Biogeosciences Discuss., https://doi.org/10.5194/bg-2018-340
Manuscript under review for journal Biogeosciences
Discussion started: 2 August 2018

Table

Table 1: Concentrations of specific Fe phases and their ratio to both total reactive Fe and total Fe at Site 973-4. Concentrations of Fe carbonates are taken from Zhang et al. (2018b).

Fe burial phase	Concentration below SMTZ (µmol g^{-1})	Concentration in SMTZ (µmol g^{-1})	Fe (II)/total reactive Fe below SMTZ	Fe (II)/total reactive Fe in SMTZ	Fe (II) /total Fe below SMTZ	Fe (II) /total Fe in SMTZ
Vivianite	129	N.A.	41%	N.A.	34%	32%
Pyrite	4	177	1%	52%		
Fe carbonates	111	54	36%	16%		
Total reactive Fe	311	341				

Biogeosciences Discuss., https://doi.org/10.5194/bg-2018-340
Manuscript under review for journal Biogeosciences
Discussion started: 2 August 2018

Figures

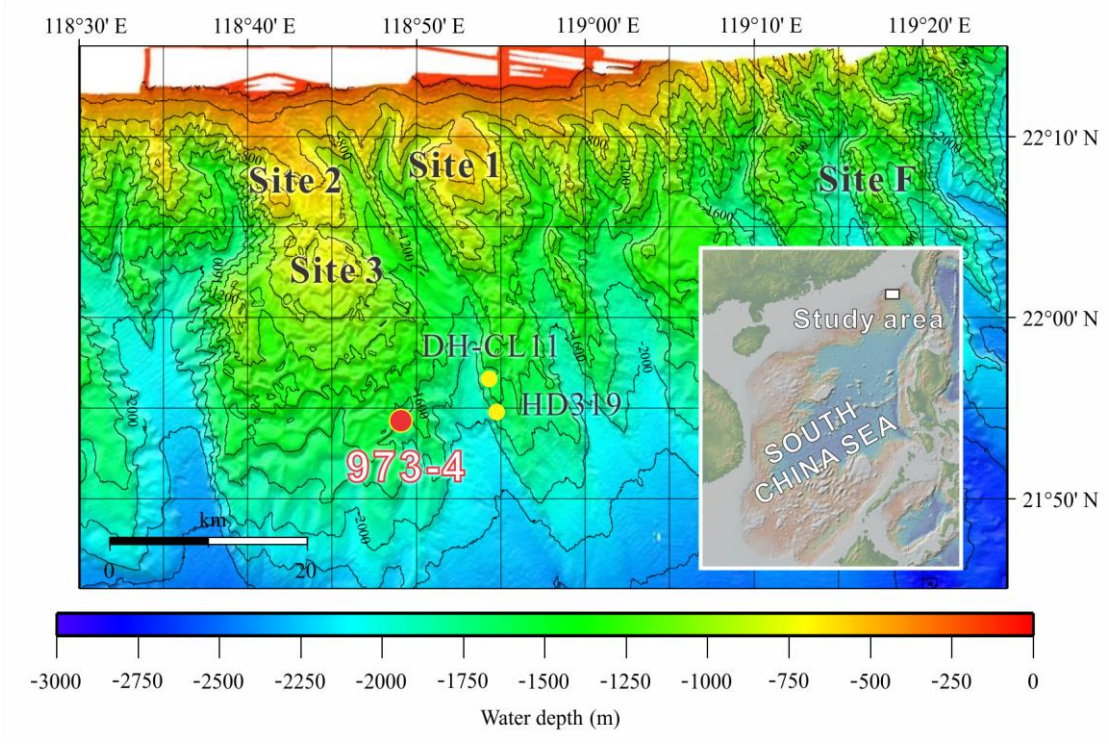

Figure 1: Bathymetric map locating Site 973-4 (red circle) with a geographical insert showing the Taixinan Basin within the wider South China Sea (after Suess et al., 2005).

Biogeosciences Discuss., https://doi.org/10.5194/bg-2018-340
Manuscript under review for journal Biogeosciences
Discussion started: 2 August 2018

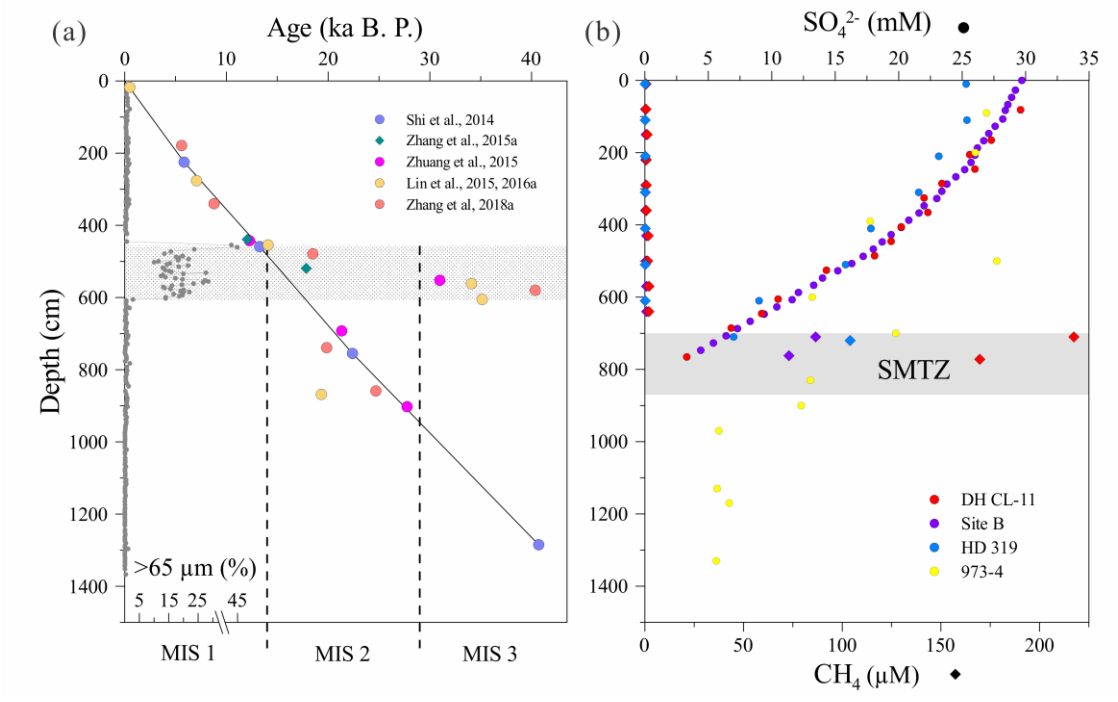

Figure 2: (a) Stratigraphic distribution of the coarse fraction (> 65 µm) and radiocarbon- or $\delta^{18}O$-derived age datums from Site 973-4. (b) Profiles of interstitial sulfate (circles) and methane (diamonds) concentrations from Site 973-4 (Zhang et al., 2014) and other adjacent Sites (Lin et al., 2017b; Lu et al., 2012; Ye et al., 2016). Age constraints are either AMS ^{14}C dates derived from planktonic foraminifera (circles) in calendar years B.P. (Lin et al., 2015, 2016a; Shi et al., 2014; Zhang et al., 2018a; Zhuang et al., 2015) or via correlation to the LR04 benthic oxygen isotope stack (diamonds; Zhang et al., 2015a). MIS—Marine isotope stage. The headspace methane concentrations from Site B and HD 319 were calculated assuming the density of the wet sediments was 1.7 g cm^{-3} (Tenzer and Gladkikh, 2014). The horizontal bars in a and b represent either the coarse layer or the SMTZ, respectively.

Biogeosciences Discuss., https://doi.org/10.5194/bg-2018-340
Manuscript under review for journal Biogeosciences
Discussion started: 2 August 2018

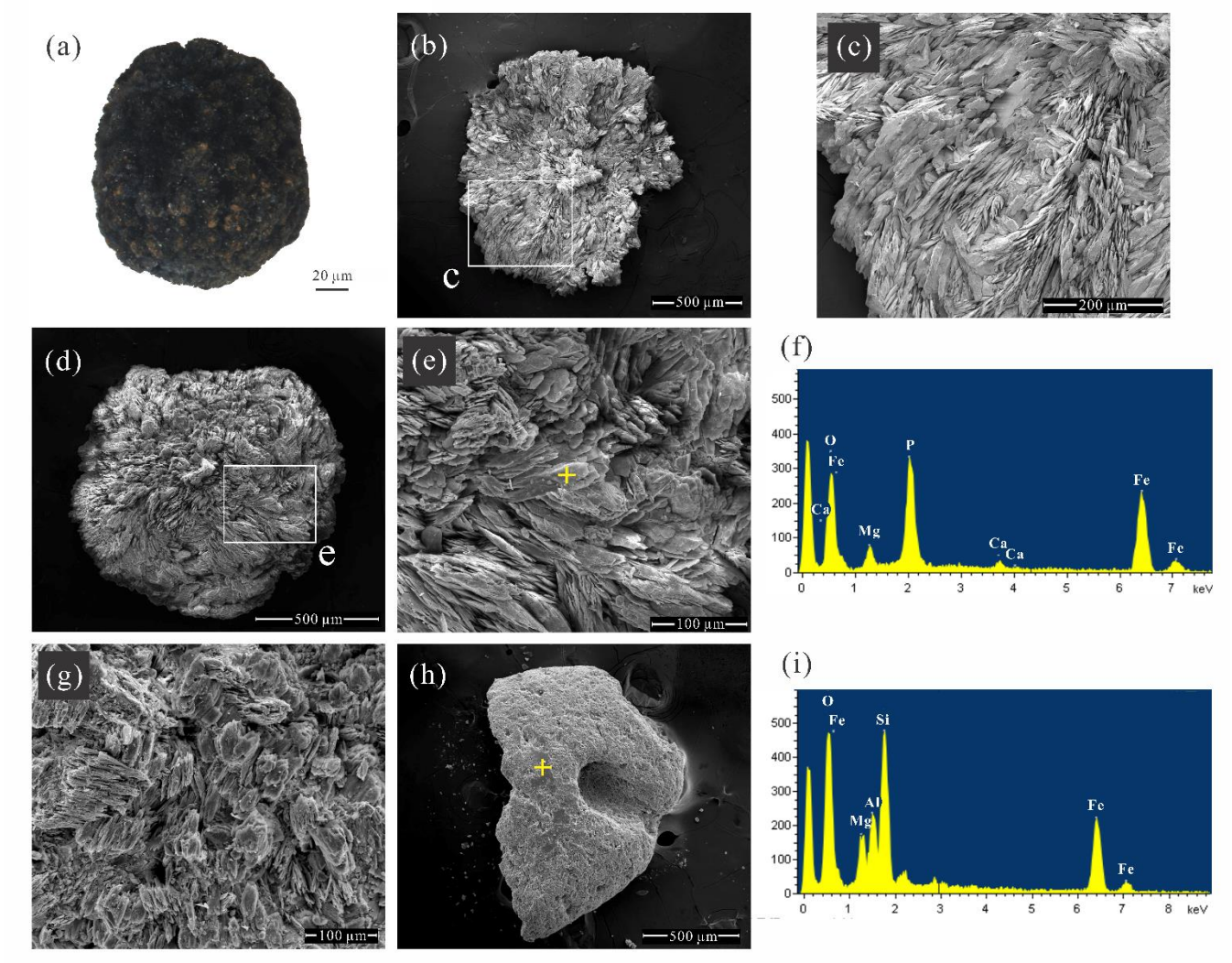

Figure 3: Images and chemical analyses of handpicked mineral aggregates from core 973-4. (a) Optical photomicrograph of an opaque dark mineral aggregate. (b−e, g) Scanning electron photomicrographs of the blue to black mineral aggregates found beneath the SMTZ. Samples b, d, g were handpicked from sediments at 1087.5, 1093.5, and 973.5 cm depth, respectively. The white boxes in b, d correspond to the fields of view enlarged c and e, respectively. (f) A spot-measurement EDS spectrum corresponding to the yellow cross in e. (h) Scanning electron photomicrograph of the grey to green mineral aggregates from sediments at 602.5 cm depth. (i) A spot-measurement EDS spectrum corresponding to the yellow cross in h.

Biogeosciences Discuss., https://doi.org/10.5194/bg-2018-340
Manuscript under review for journal Biogeosciences
Discussion started: 2 August 2018

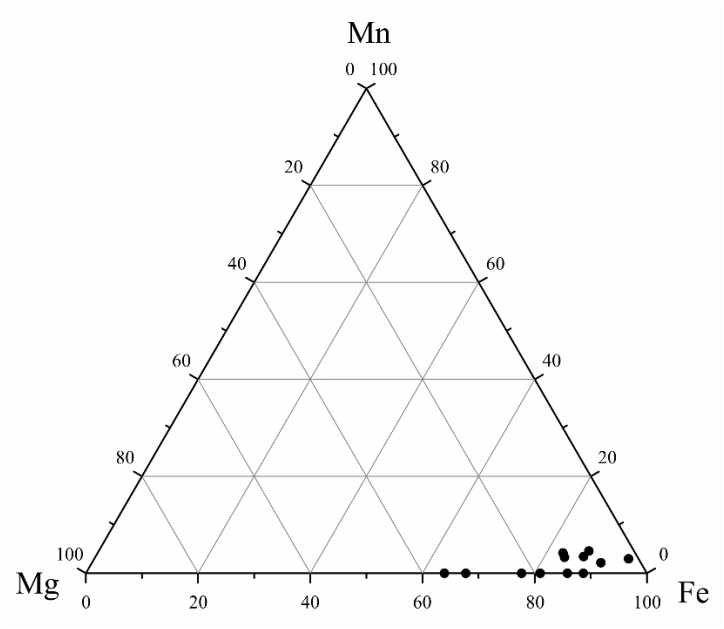

Figure 4: Ternary plot of the Fe–Mg–Mn contents (in wt.%) of the blue to black mineral aggregates isolated from sediments below the SMTZ. These data were derived from multiple EDS measurements.

Biogeosciences Discuss., https://doi.org/10.5194/bg-2018-340
Manuscript under review for journal Biogeosciences
Discussion started: 2 August 2018

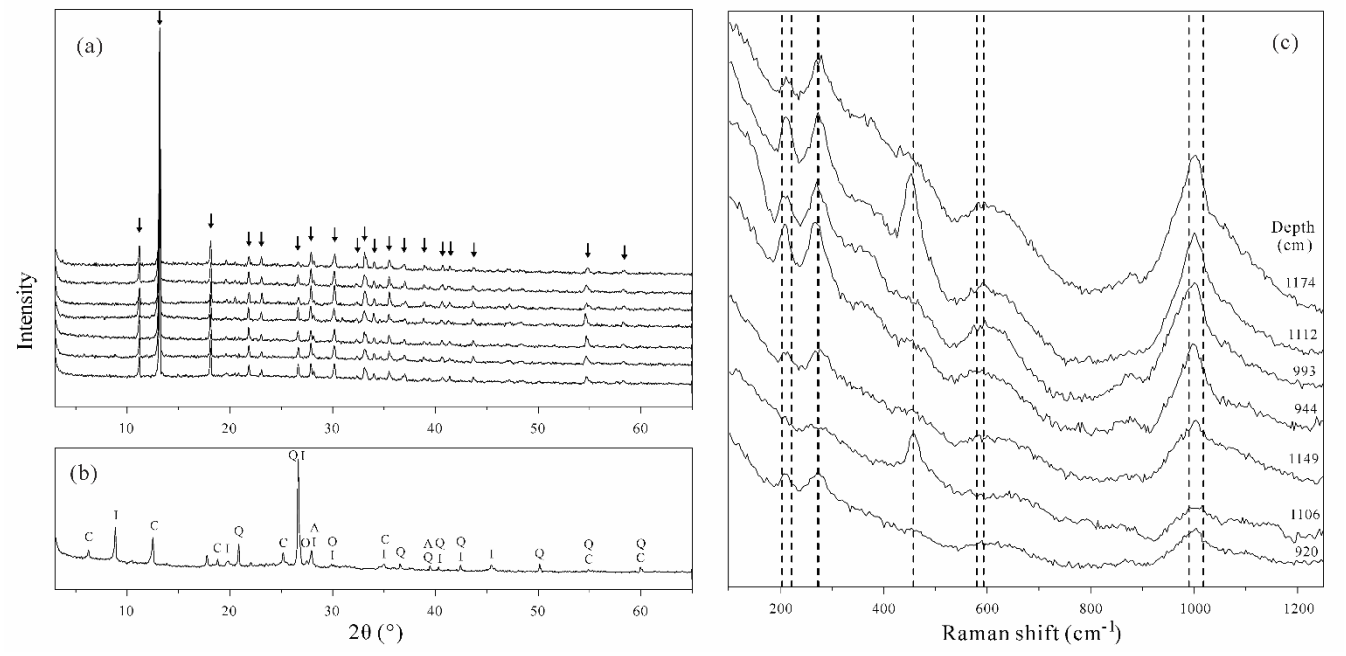

Figure 5: X-ray diffraction and Raman spectra of handpicked mineral aggregates. (a) XRD spectra of the blue to black mineral aggregates isolated from sediments from below the SMTZ. The spectra of samples from the top to the bottom correspond to samples taken at 920, 944, 993, 1106, 1112, 1149, and 1175 cm depth, respectively. All the identified peaks highlighted by arrows belong to the vivianite reference spectrum. (b) XRD spectrum of the grey to green mineral aggregates obtained from sediments at 1281 cm depth. I = illite, C = chlorites, Q = quartz, A = albite, O = orthoclase. (c) Raman spectra of the blue to black mineral aggregates from below the SMTZ. The dashed lines represent known vivianite spectral features (Piriou and Poullen, 1984).

Biogeosciences Discuss., https://doi.org/10.5194/bg-2018-340
Manuscript under review for journal Biogeosciences
Discussion started: 2 August 2018

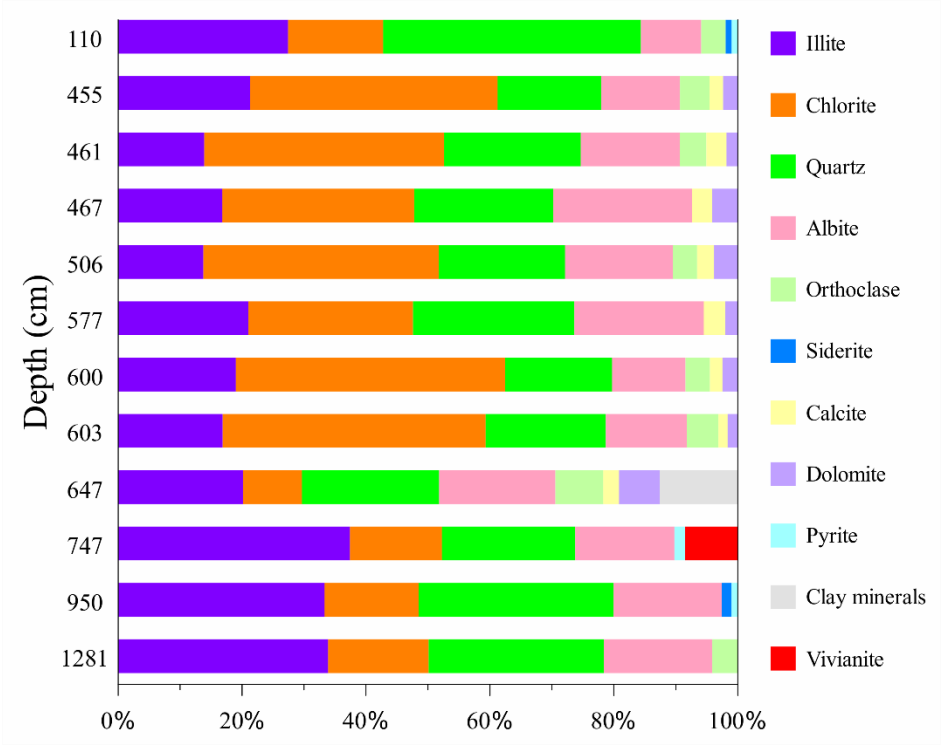

Figure 6: XRD derived depth profiles depicting the relative mineralogy of the grey to green mineral aggregates isolated from core 973-4. Some of the clay minerals from the sample at 647 cm depth remain unclassified.

Biogeosciences Discuss., https://doi.org/10.5194/bg-2018-340
Manuscript under review for journal Biogeosciences
Discussion started: 2 August 2018

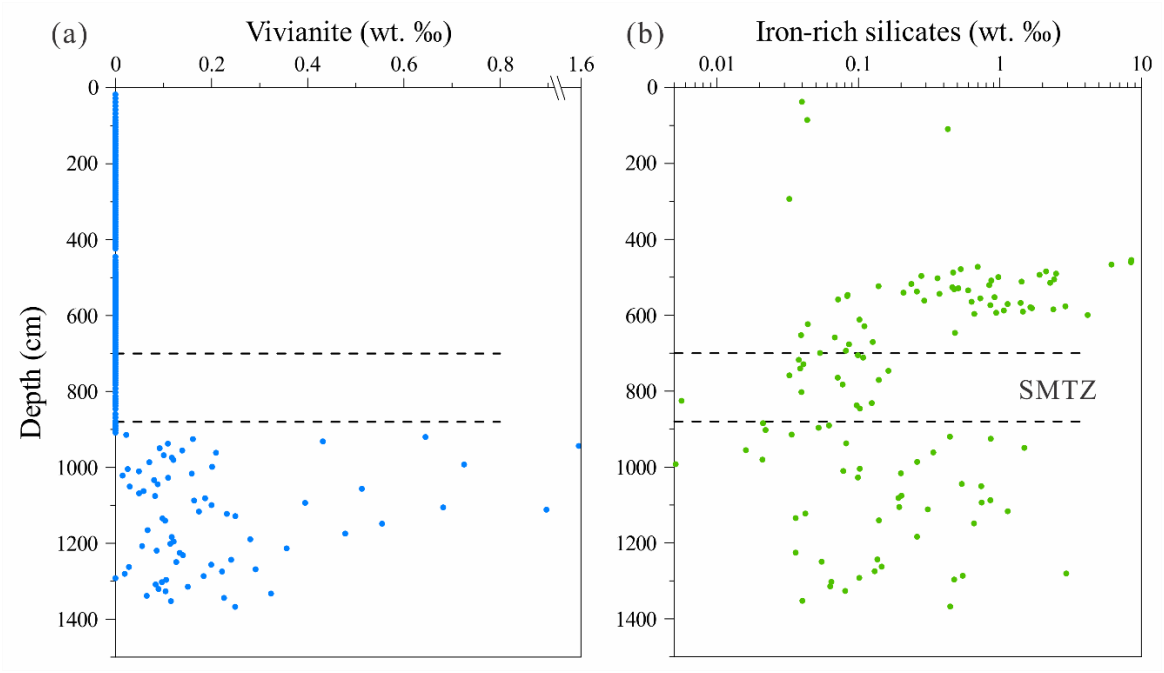

Figure 7: Depth distribution profiles of handpicked (a) vivianite, (b) Fe-rich silicates. The SMTZ is indicated by horizontal dashed lines.

Biogeosciences Discuss., https://doi.org/10.5194/bg-2018-340
Manuscript under review for journal Biogeosciences
Discussion started: 2 August 2018

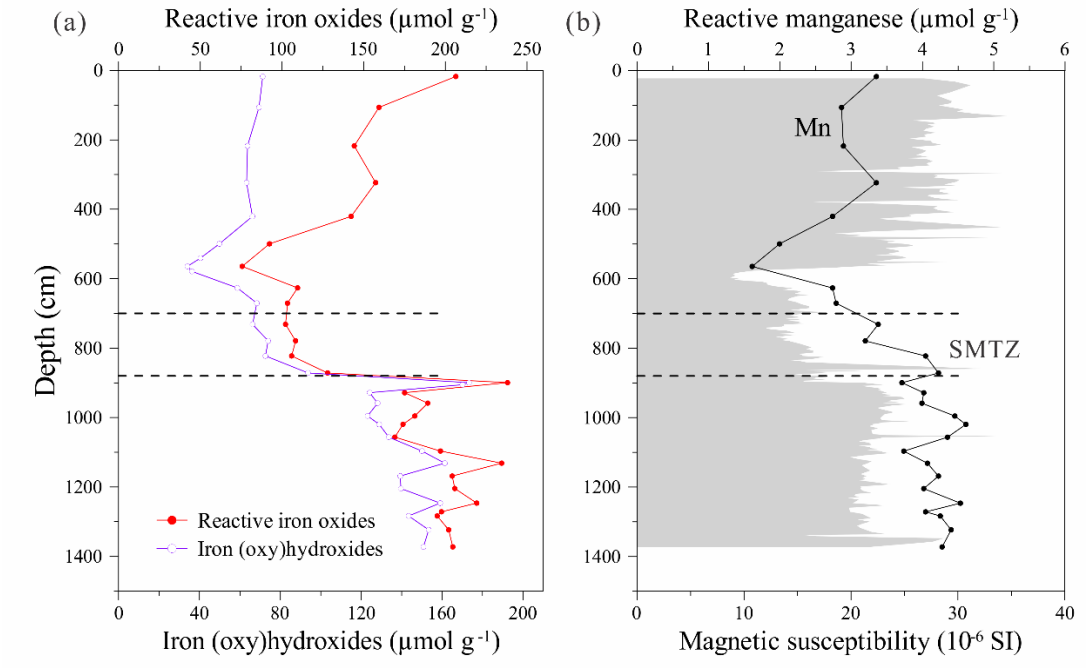

Figure 8: Depth distribution profiles of (a) Fe (oxy)hydroxides and reactive Fe-oxides, (b) reactive manganese and magnetic susceptibility. Magnetic susceptibility data are adopted from Lin et al. (2017a).

Biogeosciences Discuss., https://doi.org/10.5194/bg-2018-340
Manuscript under review for journal Biogeosciences
Discussion started: 2 August 2018

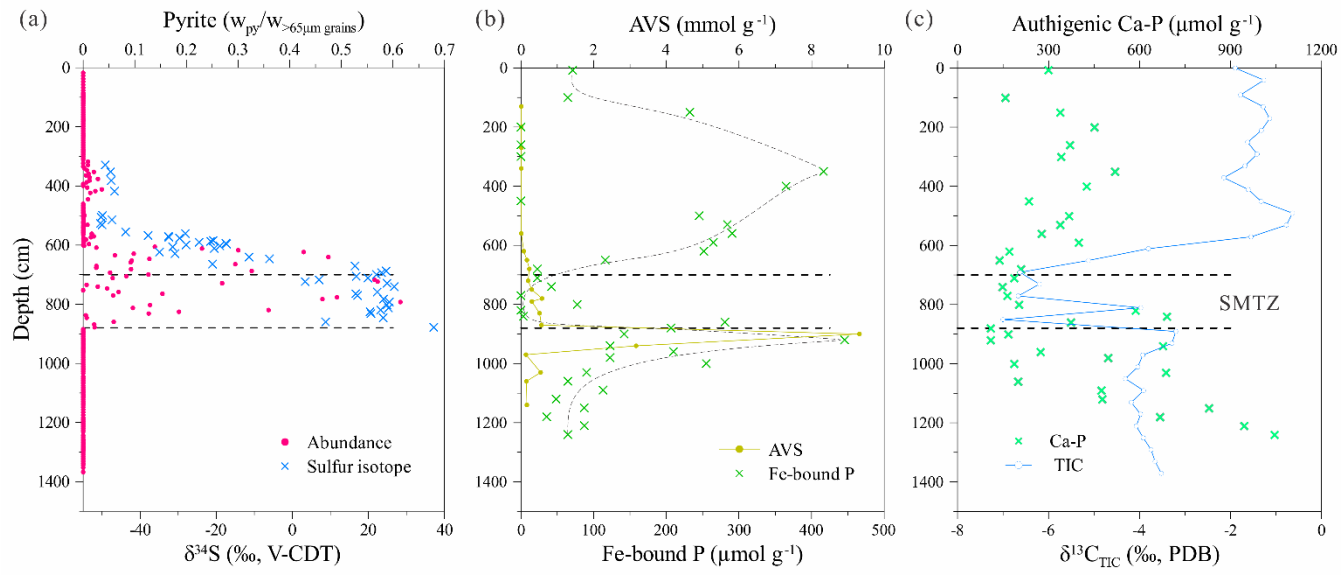

Figure 9: Depth profiles of (a) handpicked pyrite abundance and sulfur isotopic composition (Lin et al., 2015), (b) acid volatile sulfur (AVS) and Fe-bound P (Zhang et al., 2014, 2018b), (c) authigenic Ca–P and carbon isotopic composition of total inorganic carbon (TIC) (Ou, 2013; Zhang et al., 2018b).

5

Biogeosciences Discuss., https://doi.org/10.5194/bg-2018-340
Manuscript under review for journal Biogeosciences
Discussion started: 2 August 2018

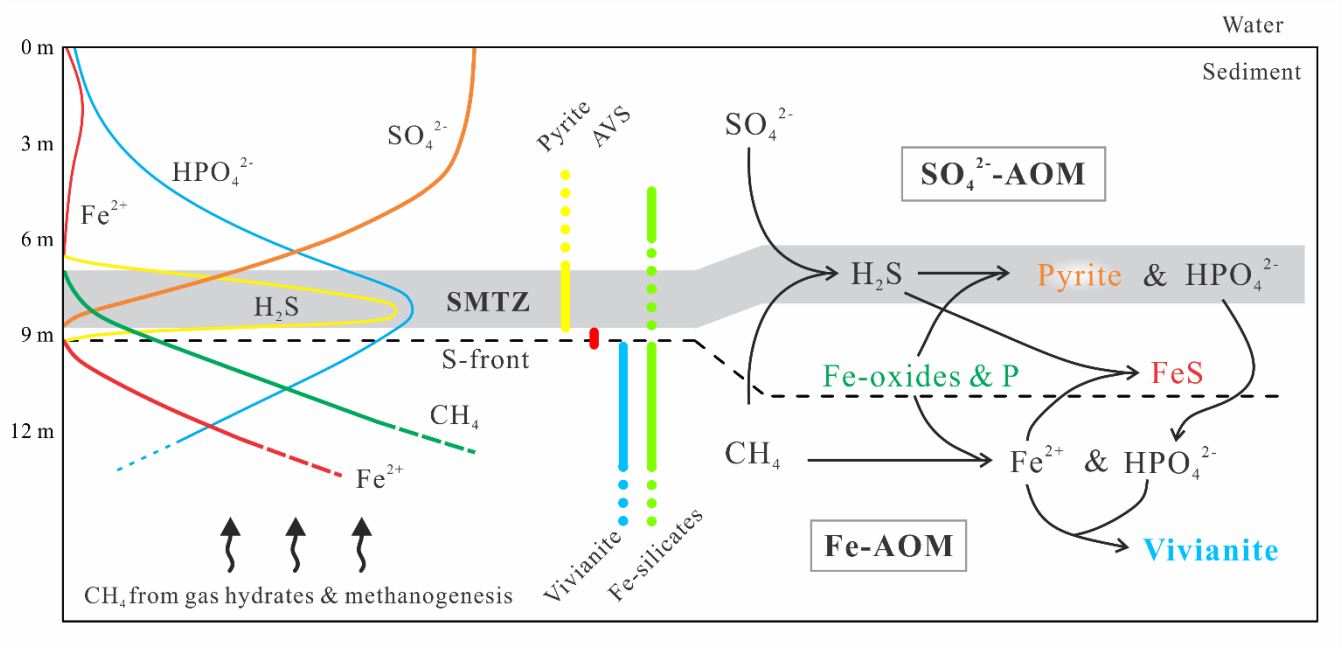

Figure 10: Schematic representation of vivianite formation below the SMTZ at Site 973-4 in the South China Sea. The left and middle parts illustrate idealized pore water and solid-phase mineral distributions. The right part illustrates the interaction between sulfate- and Fe-driven AOM coupling Fe-S-P-CH_4 cycles in proximity to the SMTZ.